



COMPUTATIONAL AEROACOUSTICS ANALYSIS OF A JET IMPINGING ON AN INCLINED PLATE

Christoph Brehm*

Co-workers: Jeff Housman[§], Cetin Kiris[§]

AMS Seminar Series at NASA Ames Research Center

*Science and Technology Corporation

[§]Applied Modeling and Simulation Branch
NASA Ames Research Center

02/05/2015

email: christoph.brehm@nasa.gov (any questions and comments are welcome!)



- Introduction to Jet Noise Source Identification and Characterization
- Computational Simulation Strategy
- Characterization of Flow Field in Source Region
- Acoustic Wave Propagation Pattern
- Noise Source Identification
 - Causality Method
 - Proper Orthogonal Decomposition
- Discussion

INTRODUCTION



- Practical examples: jet impingement during rocket launch, initial stage of launch abort, multi-stage rocket separation, jet-engine exhaust impingement, and powered Vertical Take Off and Landing (VTOL) aircraft
- Noise generation during rocket launch is a major safety concern (damage to payload and/or launch vehicle, etc.)
- Despite the wide relevance there are only few studies analyzing noise generation mechanisms for non-vertical jet impingement
- To understand noise generation for non-vertical jet impingement it is beneficial to revisit some of the methods and findings for noise generation in free jets
- Fundamental finding: Turbulent jet flows contain both fine and large-scale turbulent structures (Crow & Champagne (1971) and Brown & Roshko (1974))
- Instability-wave based models for sound generation (Morris & Tam (1979) and Tam & Burton (1984))
- Two universal spectra: “Peaky” and “broad” spectra (Tam *et al.* (1996))
large scale and fine grained turbulent structures

INTRODUCTION



- Practical examples: jet impingement during rocket launch, initial stage of launch abort, multi-stage rocket separation, jet-engine exhaust impingement, and powered Vertical Take Off and Landing (VTOL) aircraft
- Noise generation during rocket launch is a major safety concern (damage to payload and/or launch vehicle, etc.)
- Despite the wide relevance there are only few studies analyzing noise generation mechanisms for non-vertical jet impingement
- To understand noise generation for non-vertical jet impingement it is beneficial to revisit some of the methods and findings for noise generation in free jets
- Fundamental finding: Turbulent jet flows contain both fine and large-scale turbulent structures (Crow & Champagne (1971) and Brown & Roshko (1974))
- Instability-wave based models for sound generation (Morris & Tam (1979) and Tam & Burton (1984))

Physical understanding of noise sources is essential to develop acoustic models!

FREE JETS: CAUSALITY METHOD



- Noise generation mechanisms can be studied with the causality method
- Causality method involves the computation of cross-correlation between flow quantities inside the source region and acoustic pressure in the far-field
- Most direct way of identifying noise sources (Tam *et al.* (2008))
- In first applications, Rackl (1973) and Hurdle *et al.* (1974) used incompressible pressure inside the jet
- Panda & Seasholtz (2002) measured density fluctuations inside plume and cross-correlated* it with acoustic far-field measurements
 - Strong correlation from center-line of the jet downstream of potential core
- Panda *et al.* (2005) cross-correlated* additional flow quantities, such as ρ , u , v , ρu^2 , and ρv^2
 - Strongest correlation from $\langle \rho u^2; r' \rangle$
 - Larger correlations for first and third than second-order terms
- Strong correlations from large coherent flow structures

*normalized correlations were used

FREE JETS: CAUSALITY METHOD



- Bogey et al. (2007) carried out a detailed analysis of how coherent flow structures generate noise
 - Noise source is located on the center-line of the jet at the end of potential core
 - Noise is generated by periodic and intermittent intrusion of vortical structures into the jet core
- Freund (2001) showed by solving Lighthill's equation numerically that they can predict far-field noise signature
 - Source terms were provided by DNS
 - Need to account for radiating part of the source term

FREE JETS: CAUSALITY METHOD



- Bogey et al. (2007) carried out a detailed analysis of how coherent flow structures generate noise
 - Noise source is located on the center-line of the jet at the end of potential core
 - Noise is generated by periodic and intermittent intrusion of vortical structures into the jet core
- Freund (2001) showed by solving Lighthill's equation numerically that they can predict far-field noise signature
 - Source terms were provided by DNS
 - Need to account for radiating part of the source term

A good understanding of the flow field in the source region guides the interpretation of the causality analysis results.

Far-field acoustic analysis guides the placement of the field probes.

PREVIOUS STUDIES ON NON-VERTICAL JET-IMPINGEMENT



- Non-vertical jet impingement for similar flow conditions has previously been studied both numerically (Nonomura *et al.* (2011,2012), Tsutsumi *et al.* (2012,2014)) and experimentally (Nakanishi *et al.* (2012), Akamine *et al.* (2014))
- Nonomura (2011) observed at least three types of possible noise generation mechanisms:
 - (1) Mach wave radiation from turbulent jet
 - (2) Acoustic waves generated in impingement region
 - (3) Mach waves generated in wall jet
- Frequently employed empirical methods (in Eldred (1971) and Haynes & Kenny (2009)) for estimating noise signature of rocket plume do not account for second mechanism
- Nonomura & Fujii (2011) showed that the essential features responsible for noise generation appear to be insensitive of near wall turbulent structures
- Experiments by Akamine *et al.* (2014) and Nakanishi *et al.* (2012)
 - Two main propagation directions (75° and 120°)
 - 75° : Broadband peak at $St=fD/u_j \approx 0.2$
 - 120°: Peak at $St \approx 0.6$
 - Tsutsumi (2014) was able to predict OASPL within ± 5 dB employing LES

OBJECTIVE OF THE WORK

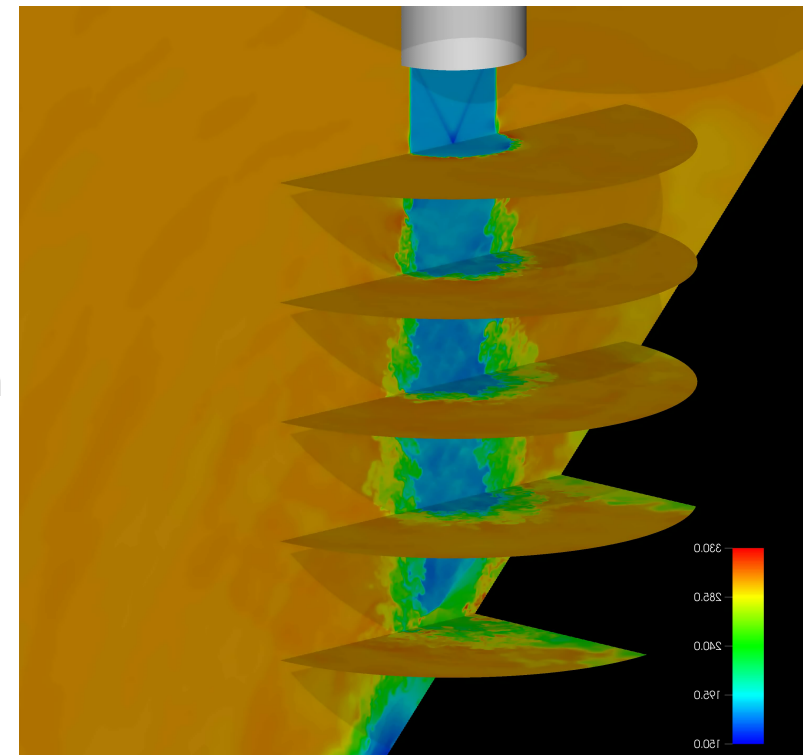


- Most dominant noise source regions have been identified in previous experimental and computational studies (1+2+3)
- Lack of detailed understanding of noise generation mechanisms
- Current paper aims at providing better physical understanding of noise generation mechanisms for a perfectly expanded jet impinging on an inclined plate

Three step approach:

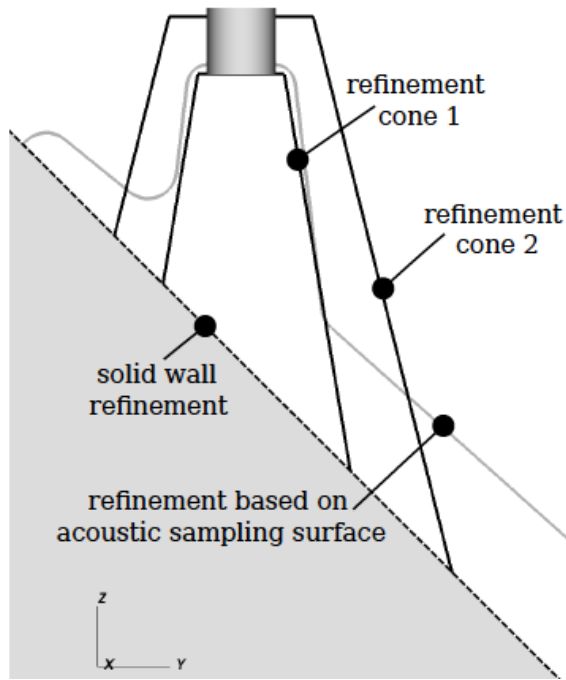
- 1.) Analyze unsteady flow in source region
- 2.) Analyze wave propagation pattern of acoustic field
- 3.) Use noise source identification/ characterization tools to connect step 1 & 2

Contours of Temperature





- Introduction to jet noise source identification and characterization
- **Computational Simulation Strategy**
- Characterization of Flow Field in Source Region
- Acoustic Wave Propagation Pattern
- Noise Source Identification
 - Causality Method
 - Proper Orthogonal Decomposition
- Discussion



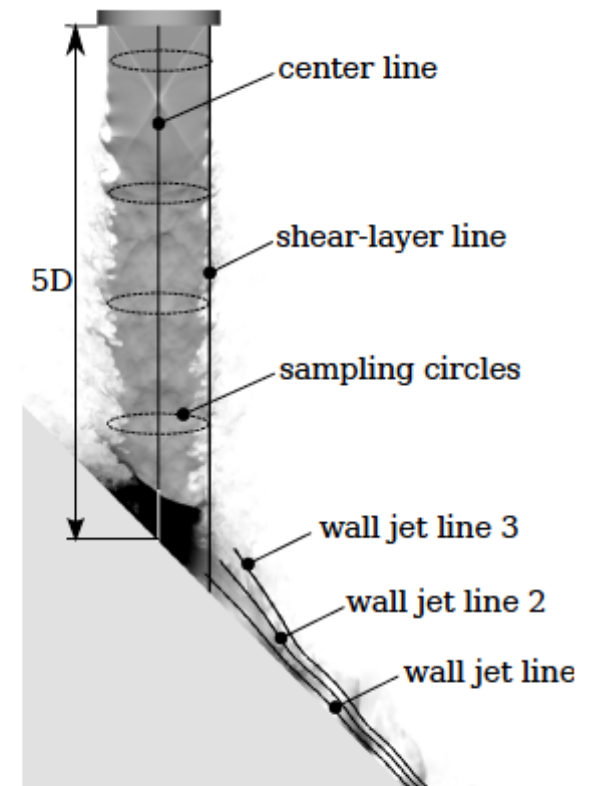
mesh refinement regions

Numerical Methods

- WENO-6 (Brehm et al. (2014) and Adams & Hu (2011))
- Viscous terms fourth-order accurate
- Explicit RK-4 for time-integration
- For more details see Kiris et al. (2014)

Computational Setup (~0.5 billion grid points)

- Two cones control grid spacing around the jet
- Acoustic sampling surface used to define grid spacing on the wall
- Grid spacing in turbulent jet is $D/\Delta x=200$ and in wall jet $D/\Delta x=100$
- “Perfectly” expanded $M=1.8$ jet, 45° inclined plate



sample points



- Some type of large eddy simulations strategy is required because DNS is not feasible for current flow conditions
- Simulation strategy with respect to nozzle inflow conditions and sub-grid scale modeling is aligned with recommendations of Shur *et al.* (2005a,b)
- Use ILES: relies on inherent regularization mechanism through truncation error of the convective fluxes (implicit SGS model (Hu & Adams (2011)))
- Used modified sixth-order accurate WENO scheme (Hu *et al.* (2010) and Brehm *et al.* (2014))
 - Hu & Adams (2011) demonstrated superior physically motivated scale separation properties of mod. WENO-6
- Modeled incoming nozzle boundary layer with RANS precursor calculations to estimate displacement thickness of boundary layer
- No inflow forcing needed because impinging jet generates elevated background noise level; eliminates dependence on free parameters
- Grid convergence study in Brehm *et al.* (2013) and Housman *et al.* (2013)

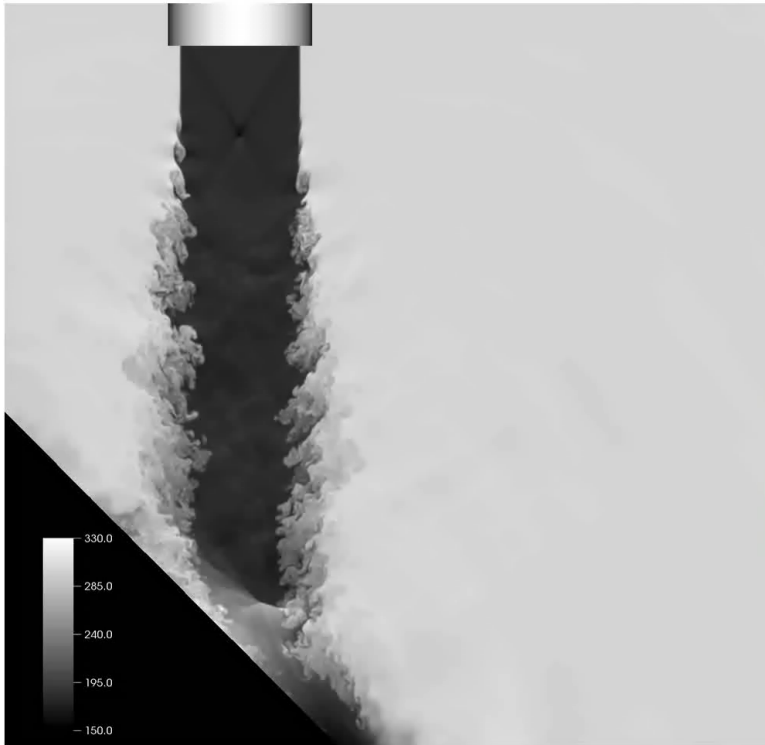


- Introduction to jet noise source identification and characterization
- Computational Simulation Strategy
- Characterization of Flow Field in Source Region
- Acoustic Wave Propagation Pattern
- Noise Source Identification
 - Causality Method
 - Proper Orthogonal Decomposition
- Discussion

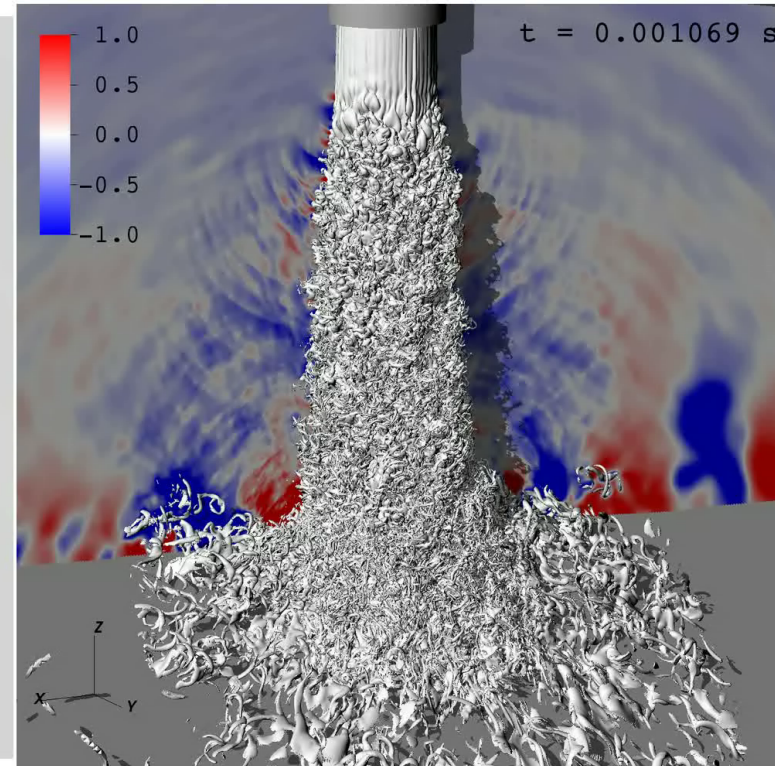
FLOW VISUALIZATION



Contours of Temperature



Q-criterion and Gauge Pressure

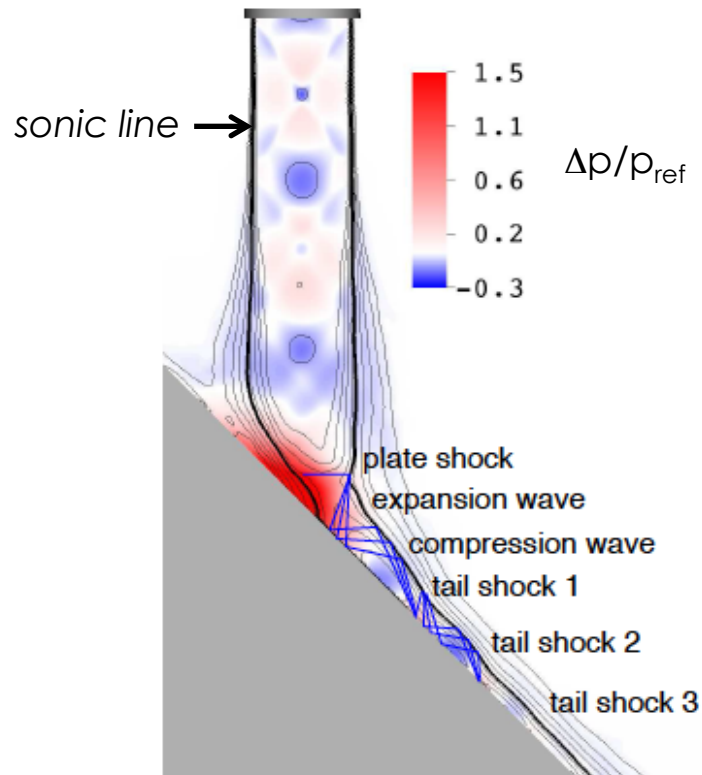


- To identify and characterize noise generation mechanisms it is important to carefully examine the source region and the acoustic field (causality)
- Experiments did not observe feedback for 45°
- (1) Jet quickly goes through complicated transition process, (2) turbulent shear layer thickens in downstream direction, (3) potential core length $\sim 8D$, (4) coherent flow structures can survive the interactions in the impingement zone and convect with the wall jet

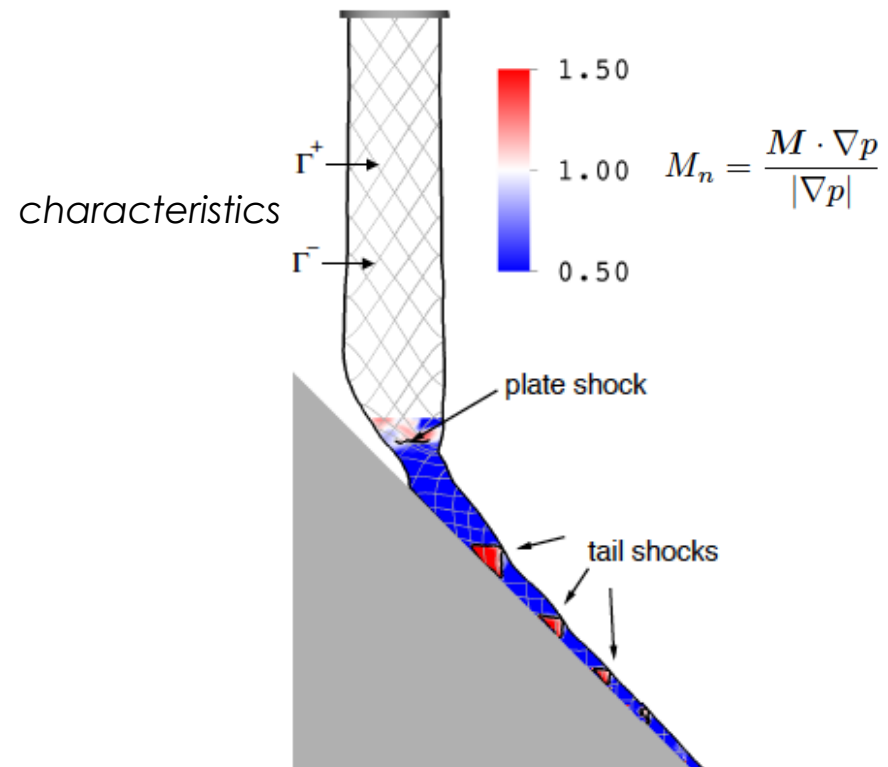
MEAN FLOW FEATURES



Illustration of compression and expansion waves



Normal Mach number contours

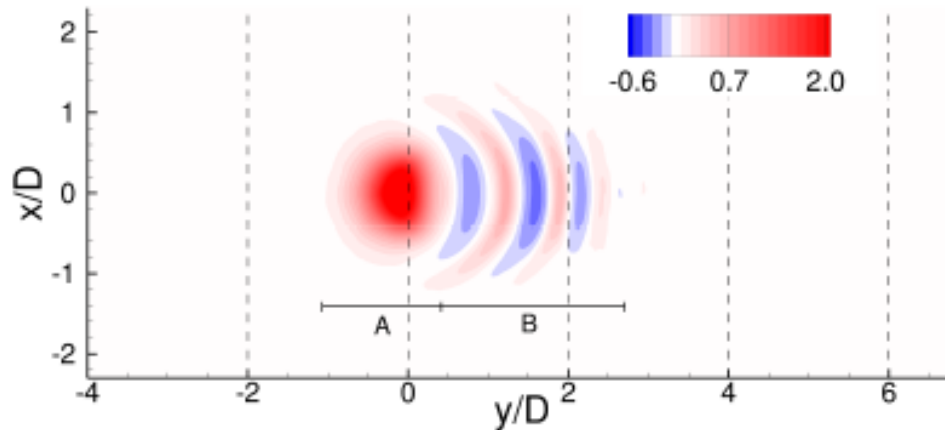


- Mean flow provides general idea about possible interactions
- Mild over-expansion ($\sim 0.5\%$ in pressure)
- Plate and tail shocks can clearly be identified
- Interaction of coherent flow structures with tail shocks are relevant for noise generation

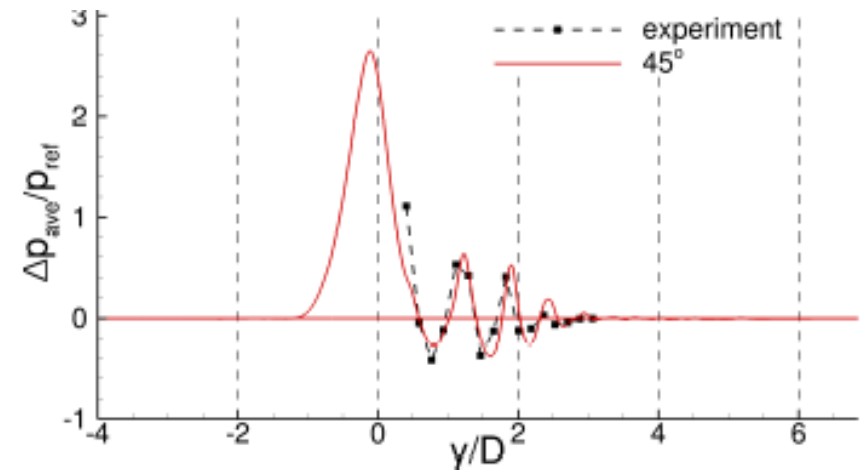
COMPARISON WITH EXPERIMENTS



pressure on impingement plate



pressure distribution on centerline

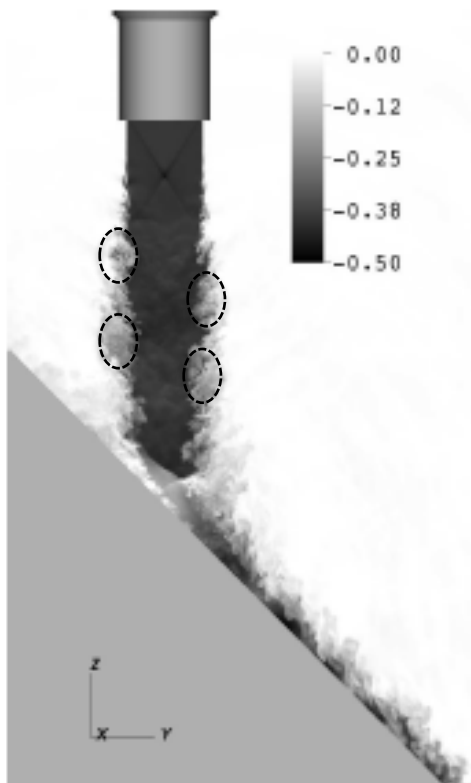


- Peak offset by $\Delta y \approx 0.1$ (also reported in hybrid LES by Tsutsumi (2014))
- Good agreement with limited experimental data
- Collaboration with JAXA
- Conditions based on experiments by Nakanishi et al. (2012) and Akamine et al. (2014) at the UT-Kashiwa hypersonic and high-temperature wind tunnel

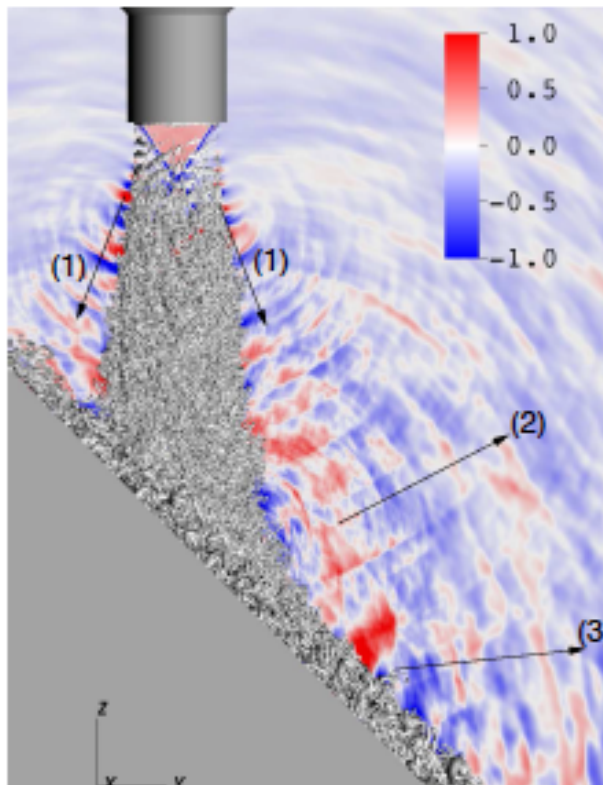
UNSTEADY FLOW FEATURES



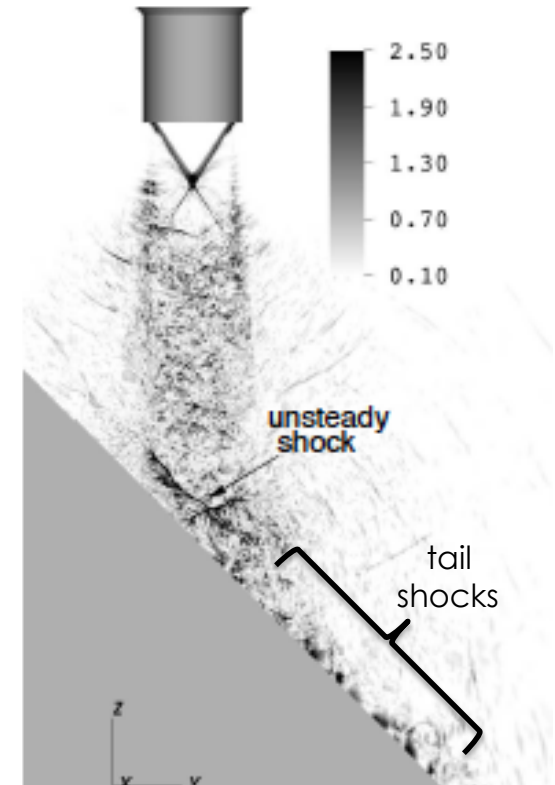
gray-scale contours of temperature



Q-criterion and gauge pressure



dilatation contours

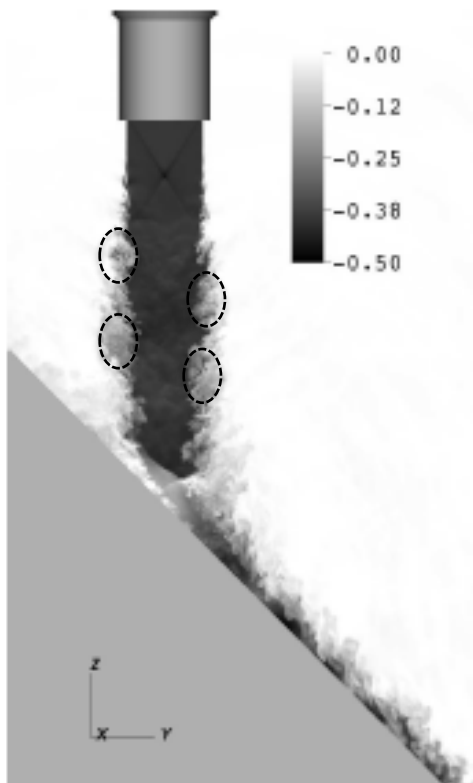


- Wide range of relevant scales
- Small grained turbulent structures and small eddies agglomerated
- Unsteady plate and tail shocks

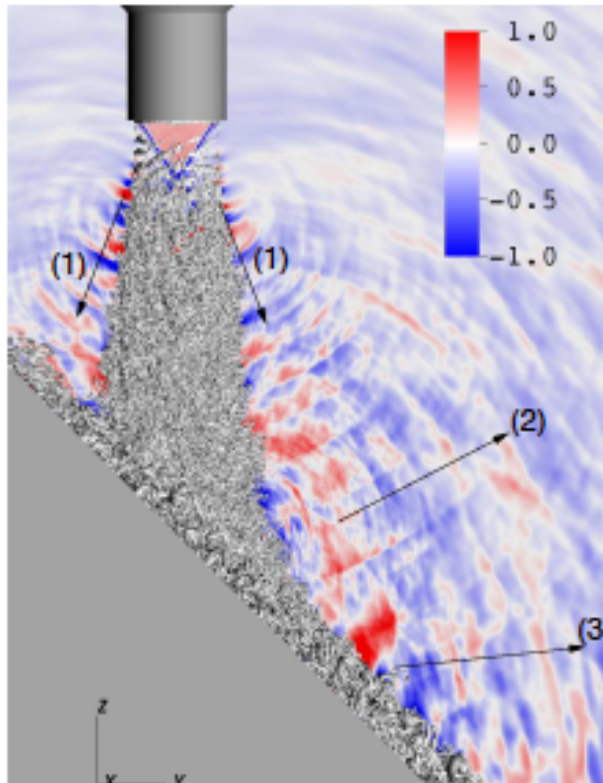
UNSTEADY FLOW FEATURES



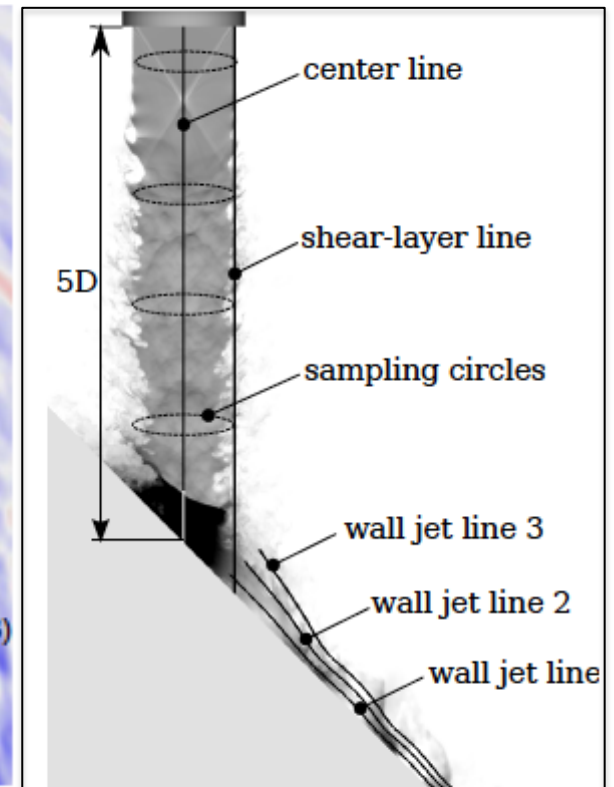
gray-scale contours of temperature



Q-criterion and gauge pressure



sampling points

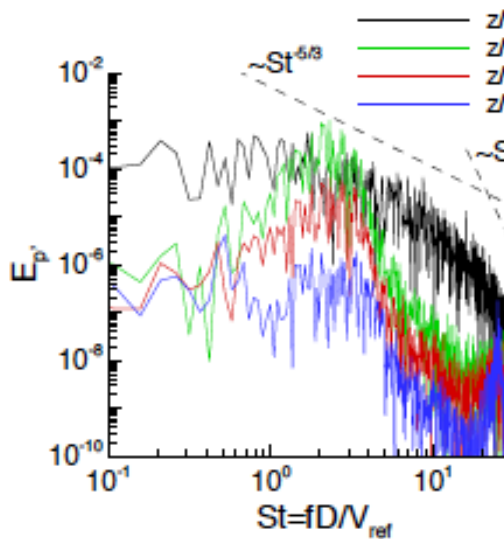


- Wide range of relevant scales
- Small grained turbulent structures and small eddies agglomerated
- Unsteady plate and tail shocks

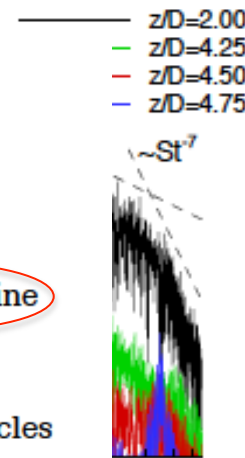
UNSTEADY FLOW FEATURES



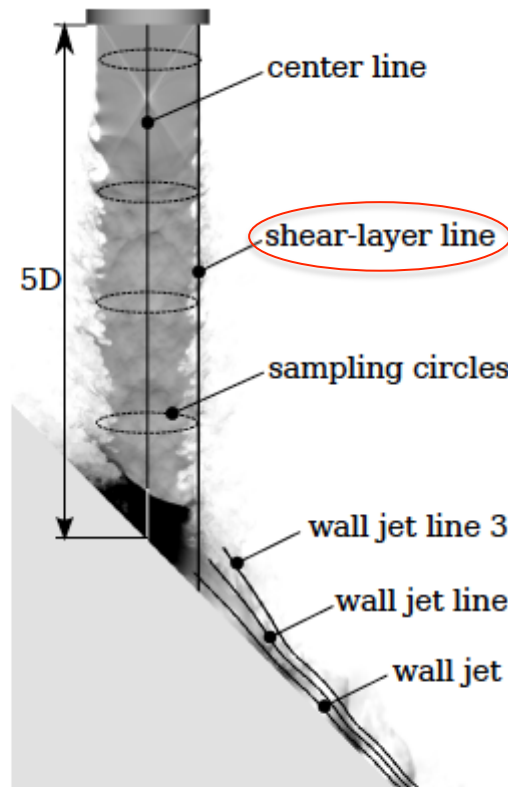
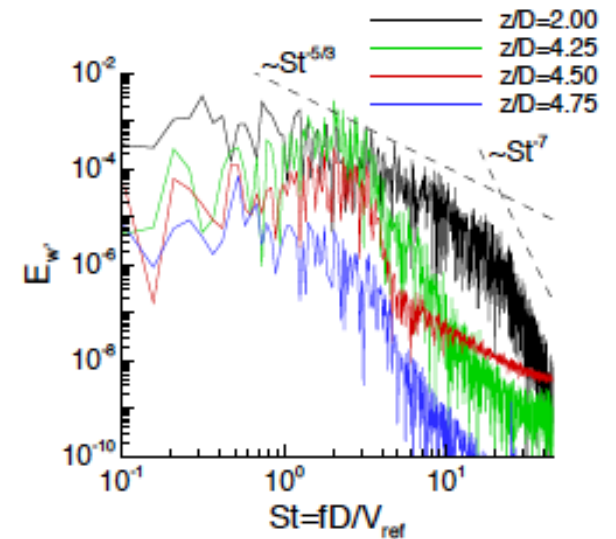
power spectra of disturbance pressure



Power spectra of v'-velocity



Power spectra of w'-velocity

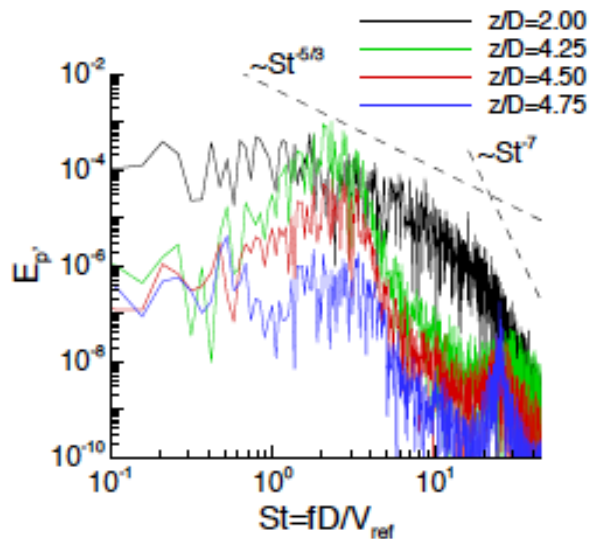


- Transition initiated
 - Flow along shear
 - Spectra seem to
 - Frequencies converged up to roughly $St \approx 5$
 - Convergence study in Housman et al. (2013) and Brehm et al. (2013)
-)
- "turbulent" at $z/D \approx 4$
- avior in inertial sub-range ($\sim St^{-5/3}$)

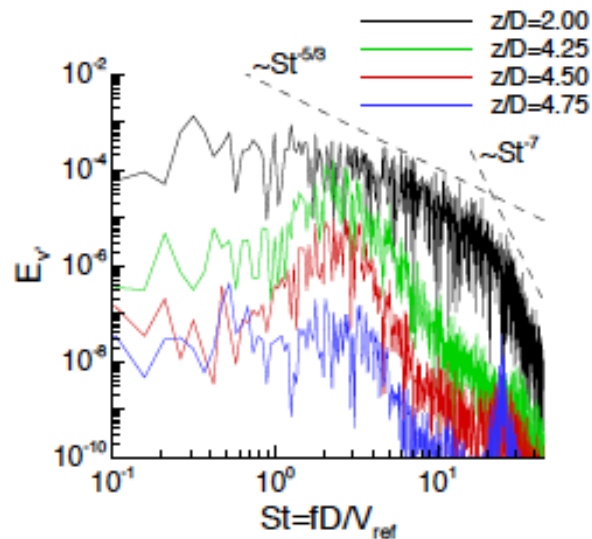
UNSTEADY FLOW FEATURES



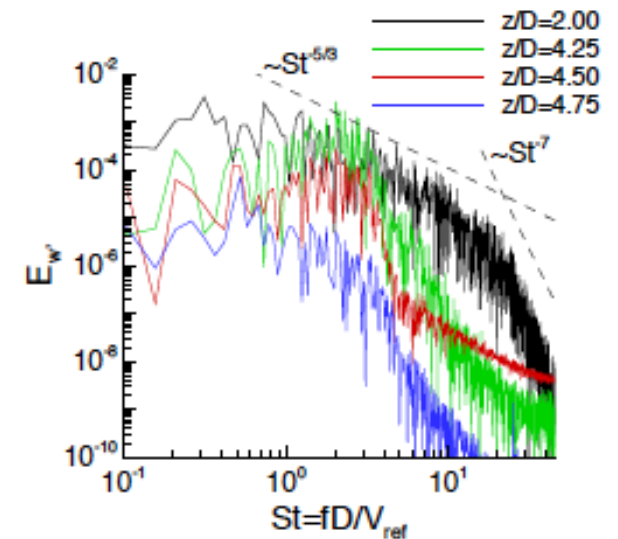
power spectra of disturbance pressure



Power spectra of v' -velocity

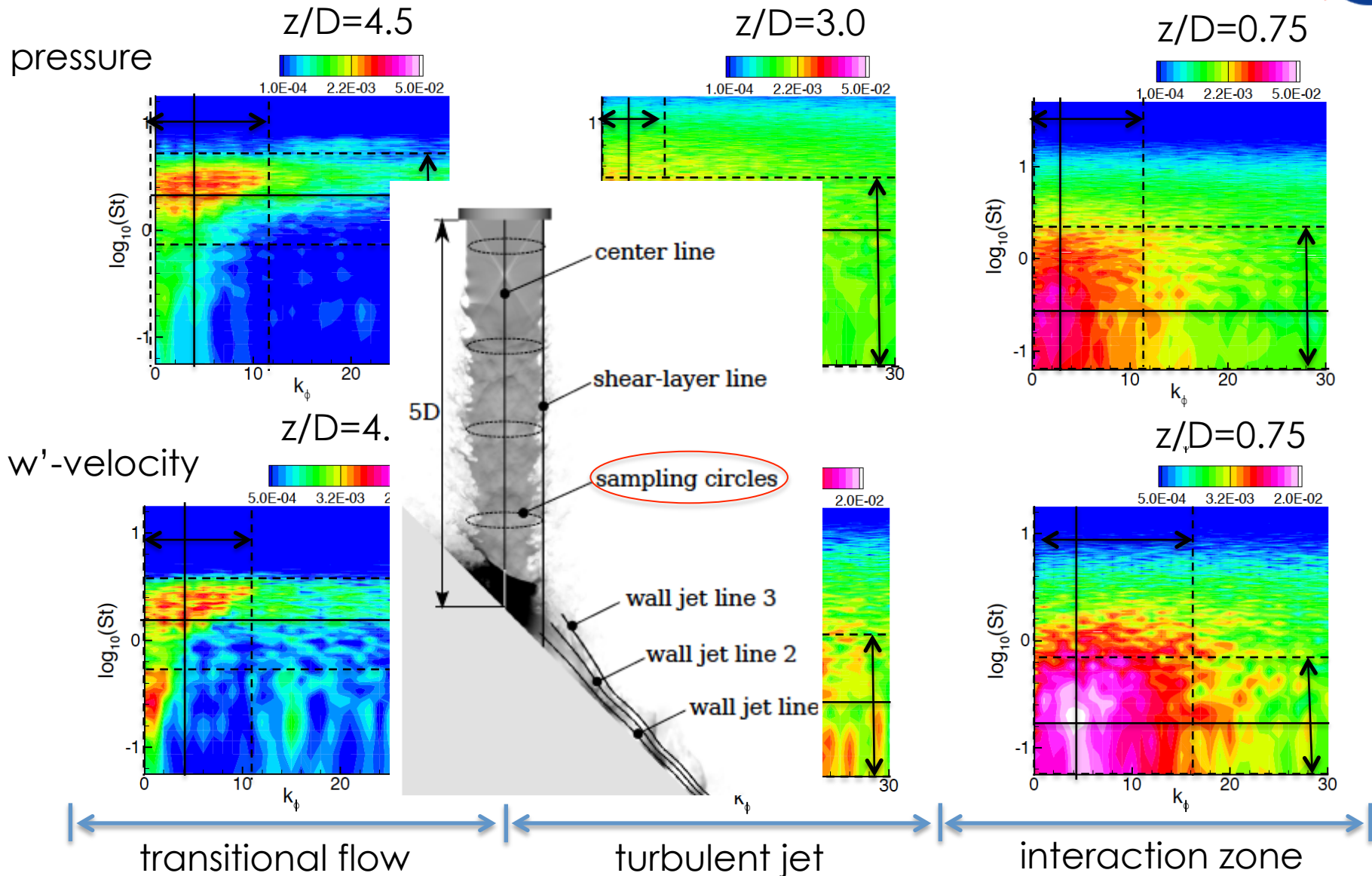


Power spectra of w' -velocity



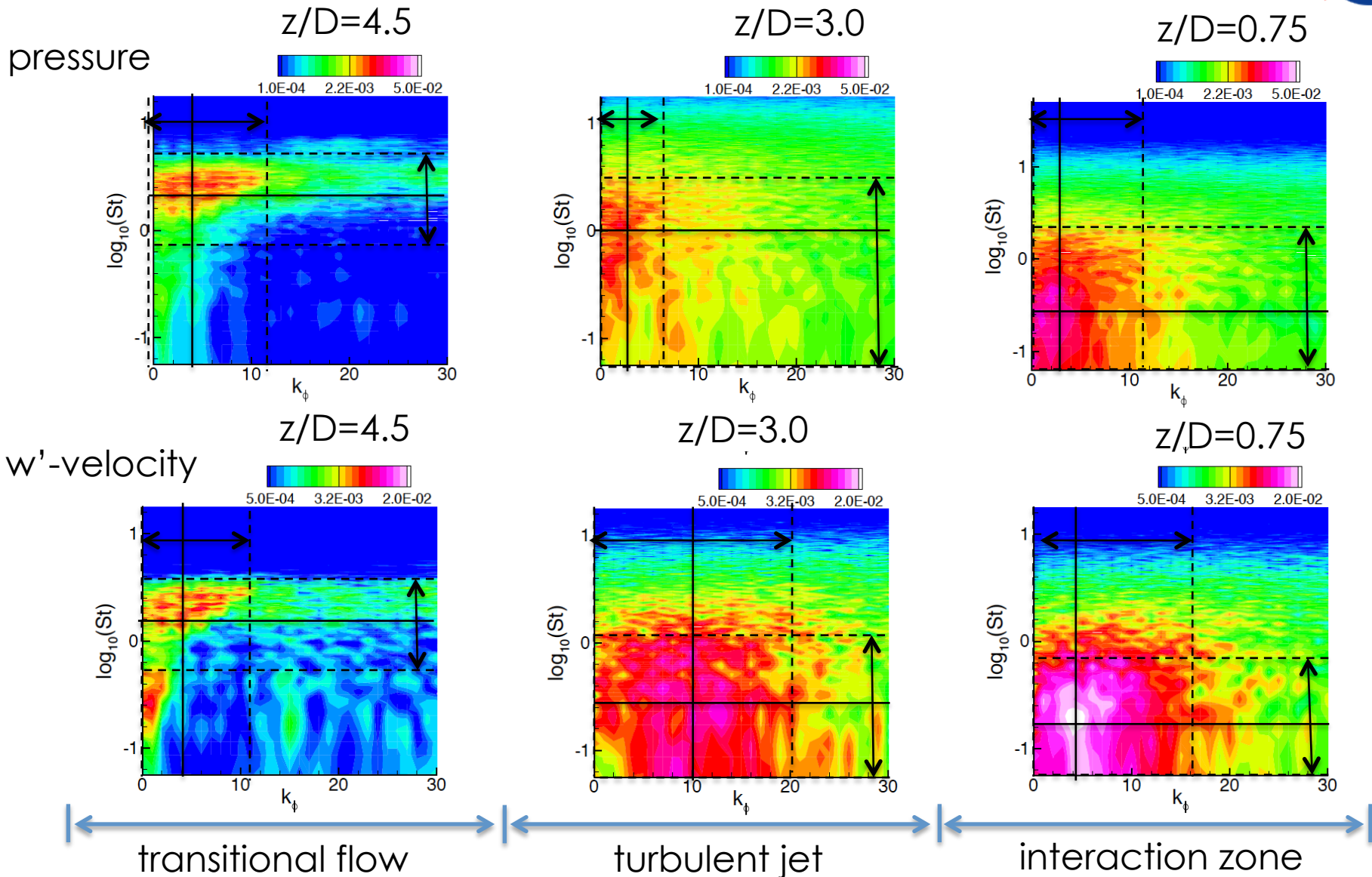
- Transition initiated in shear layer for $St \approx O(1)$
- Flow along shear layer line is considered “turbulent” at $z/D \approx 4$
- Spectra seem to capture asymptotic behavior in inertial sub-range ($\sim St^{-5/3}$)
- Frequencies converged up to roughly $St \approx 5$
- Convergence study in Housman et al. (2013) and Brehm et al. (2013)

FROM NOZZLE EXIT TO IMPINGEMENT POINT



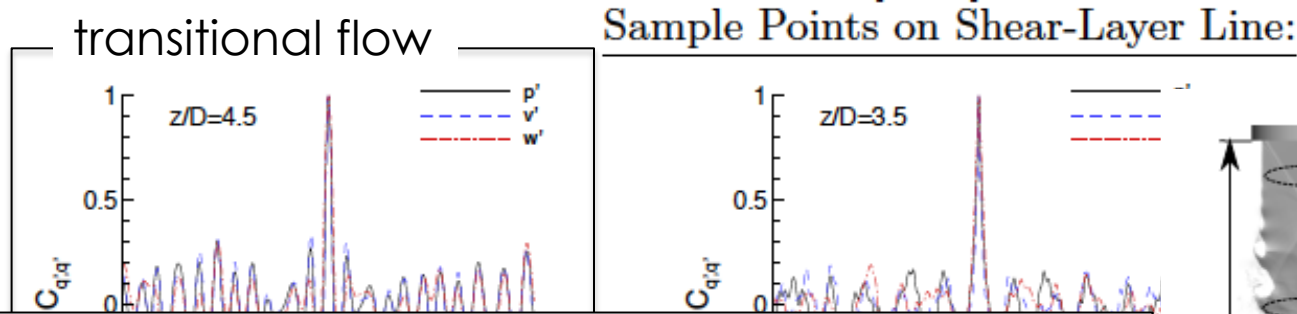
- Differences in the spectra are important for noise source identification

FROM NOZZLE EXIT TO IMPINGEMENT POINT



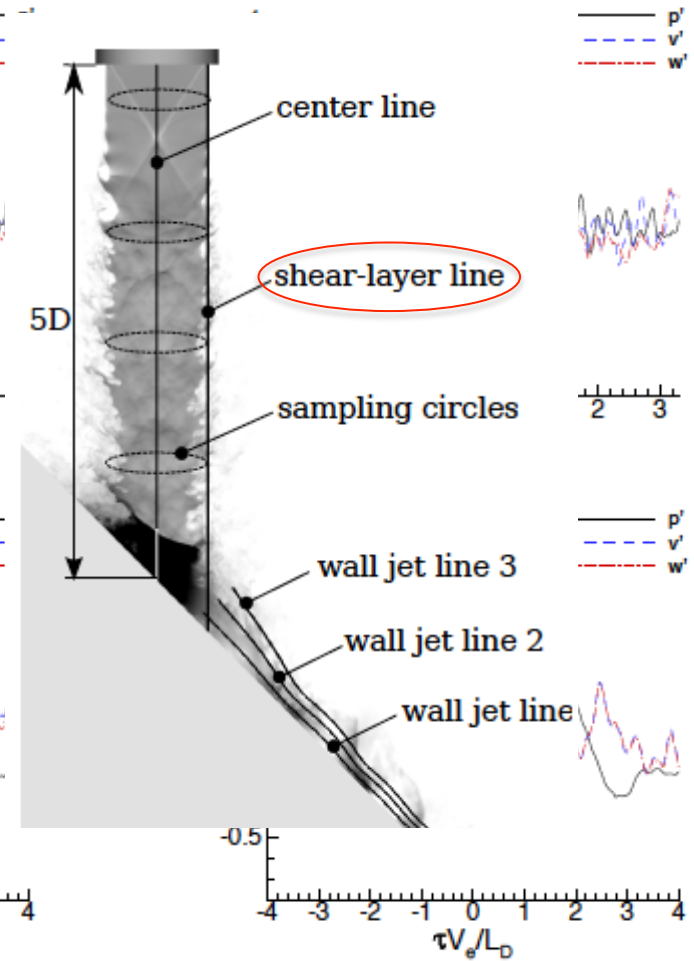
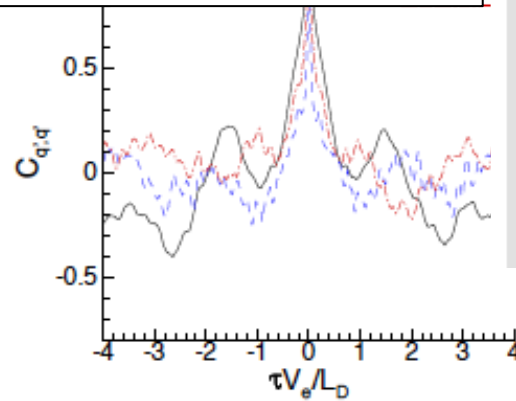
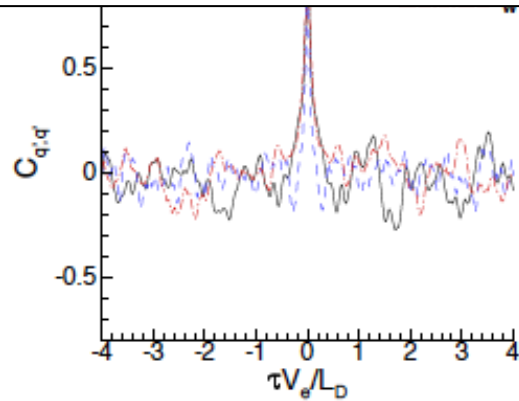
- Differences in the spectra are important for noise source identification

AUTO-CORRELATIONS



Auto-correlations and cross-correlations address:

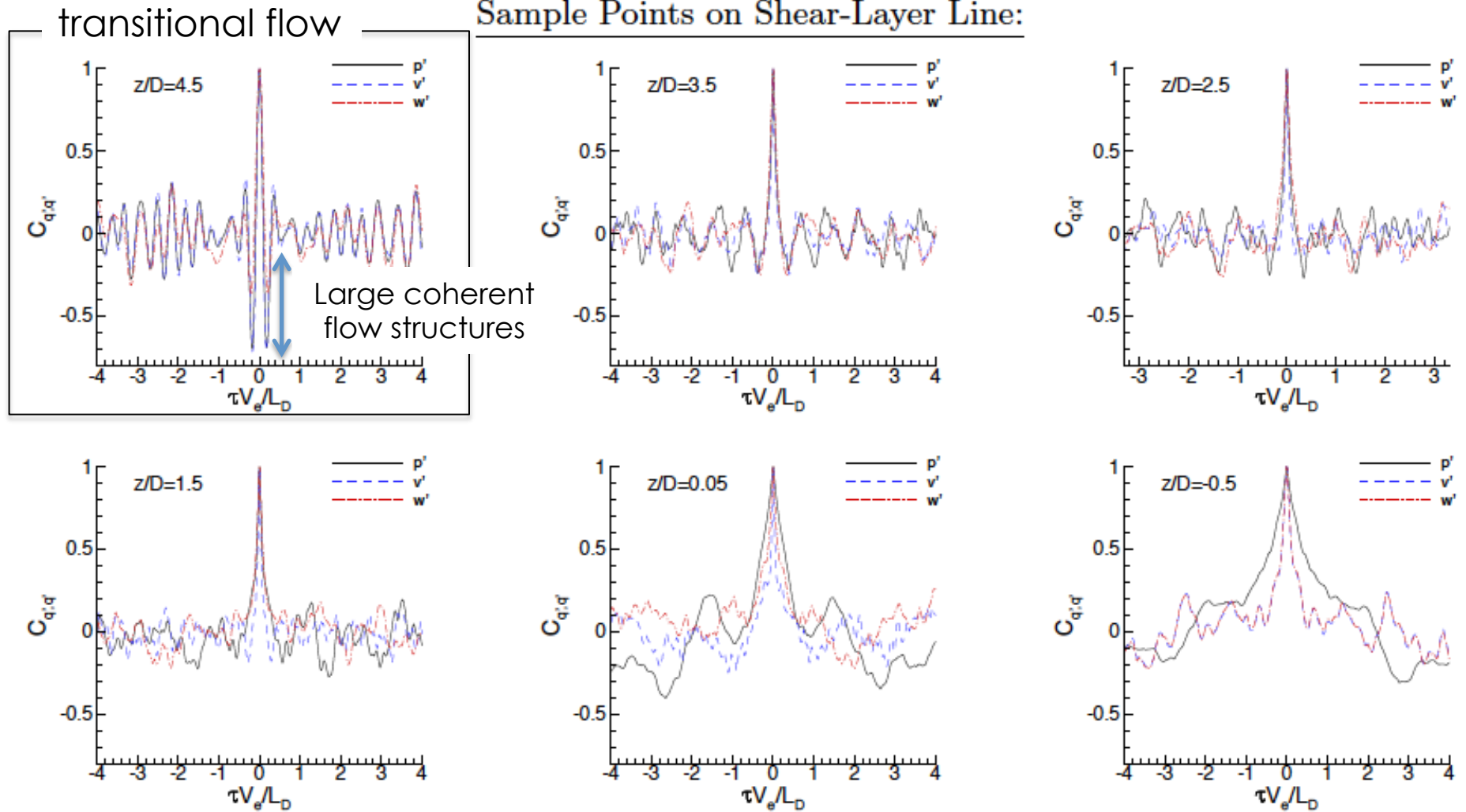
- 1.) Temporal and “streamwise” length scales
- 2.) Disparity in scales (shear layer vs. jet axis)
- 3.) Relationship between flow quantities



AUTO-CORRELATIONS



Sample Points on Shear-Layer Line:



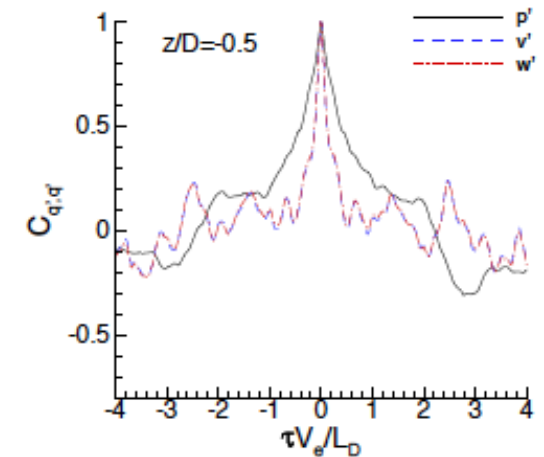
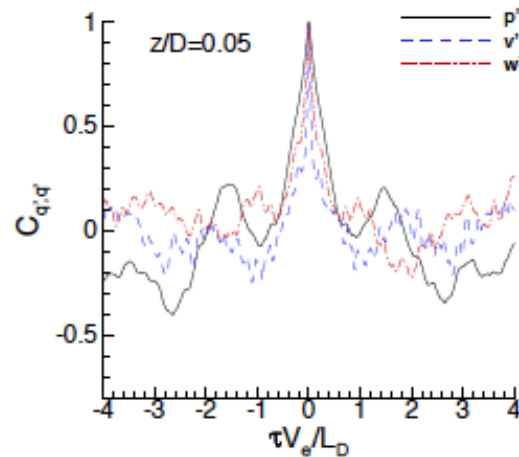
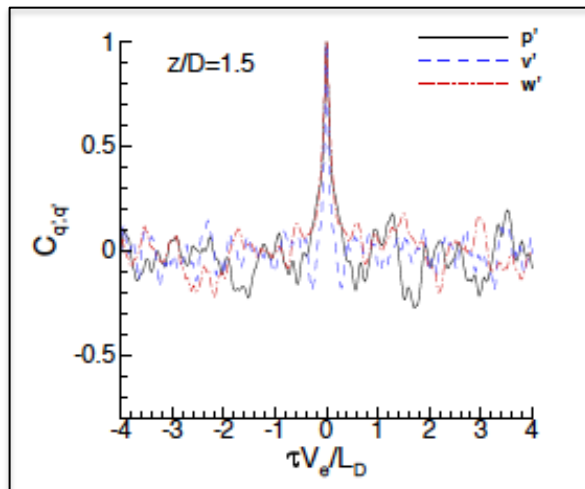
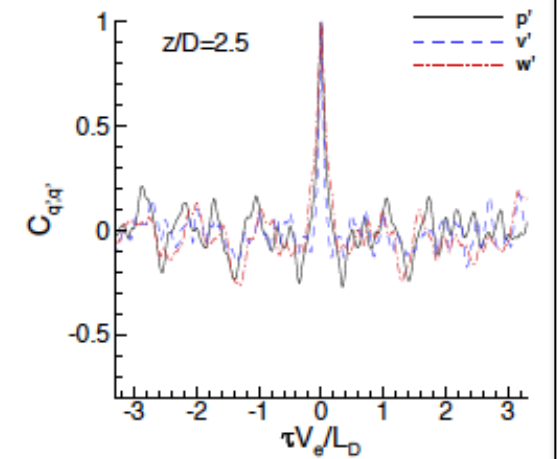
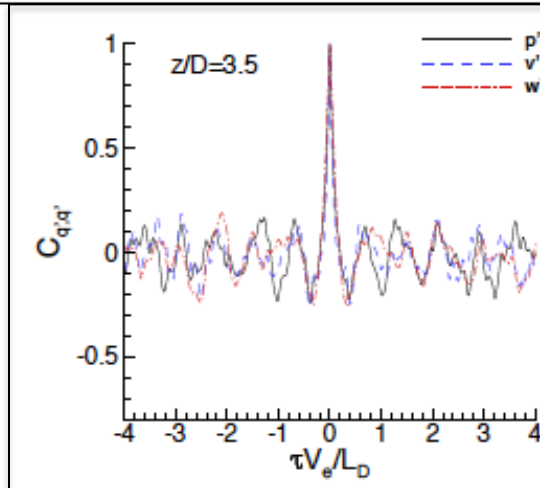
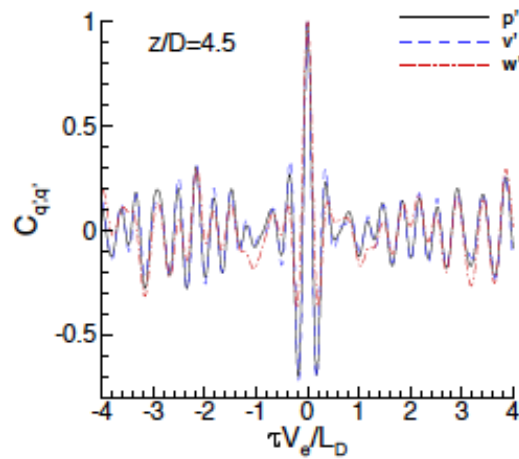
- Auto-correlations can be used to compare temporal length scales
- Convert into physical length scale with local convection speed

AUTO-CORRELATIONS



Sample Points on Shear-Layer Line:

turbulent jet

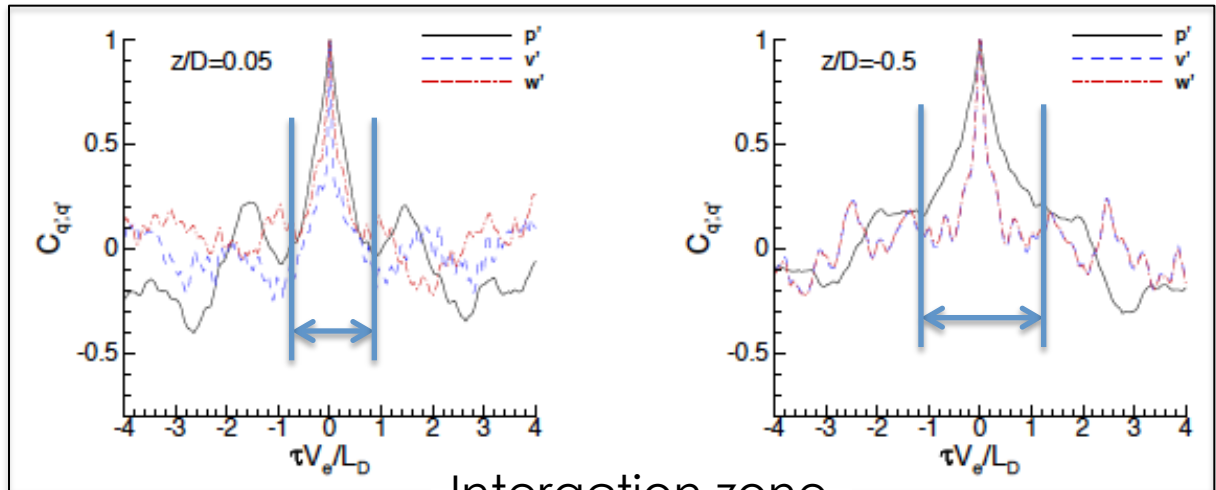
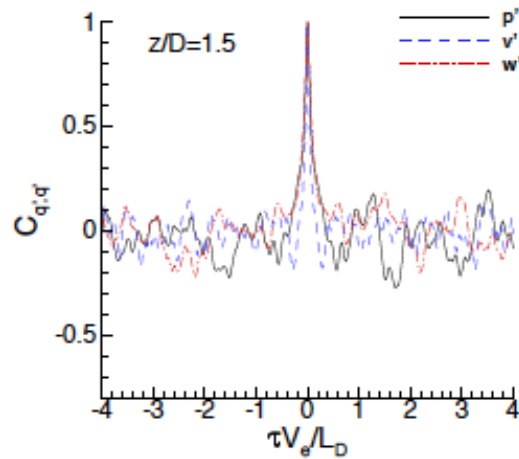
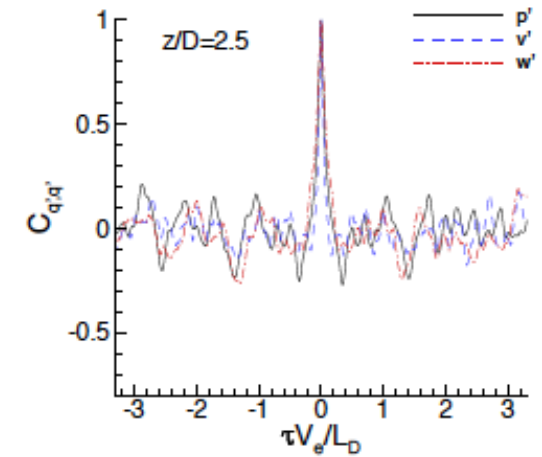
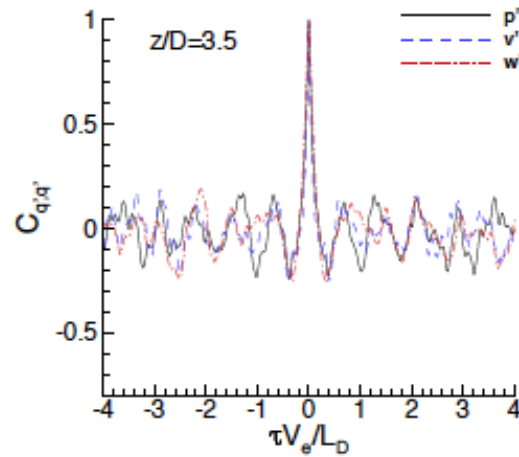
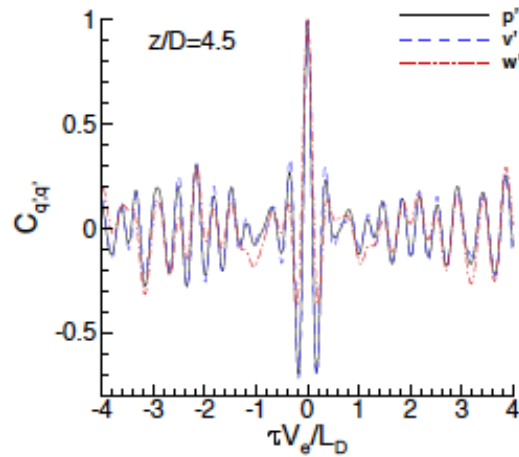


- Deep undershoot disappears due to randomization
- Increase width of peak indicates larger scales

AUTO-CORRELATIONS



Sample Points on Shear-Layer Line:



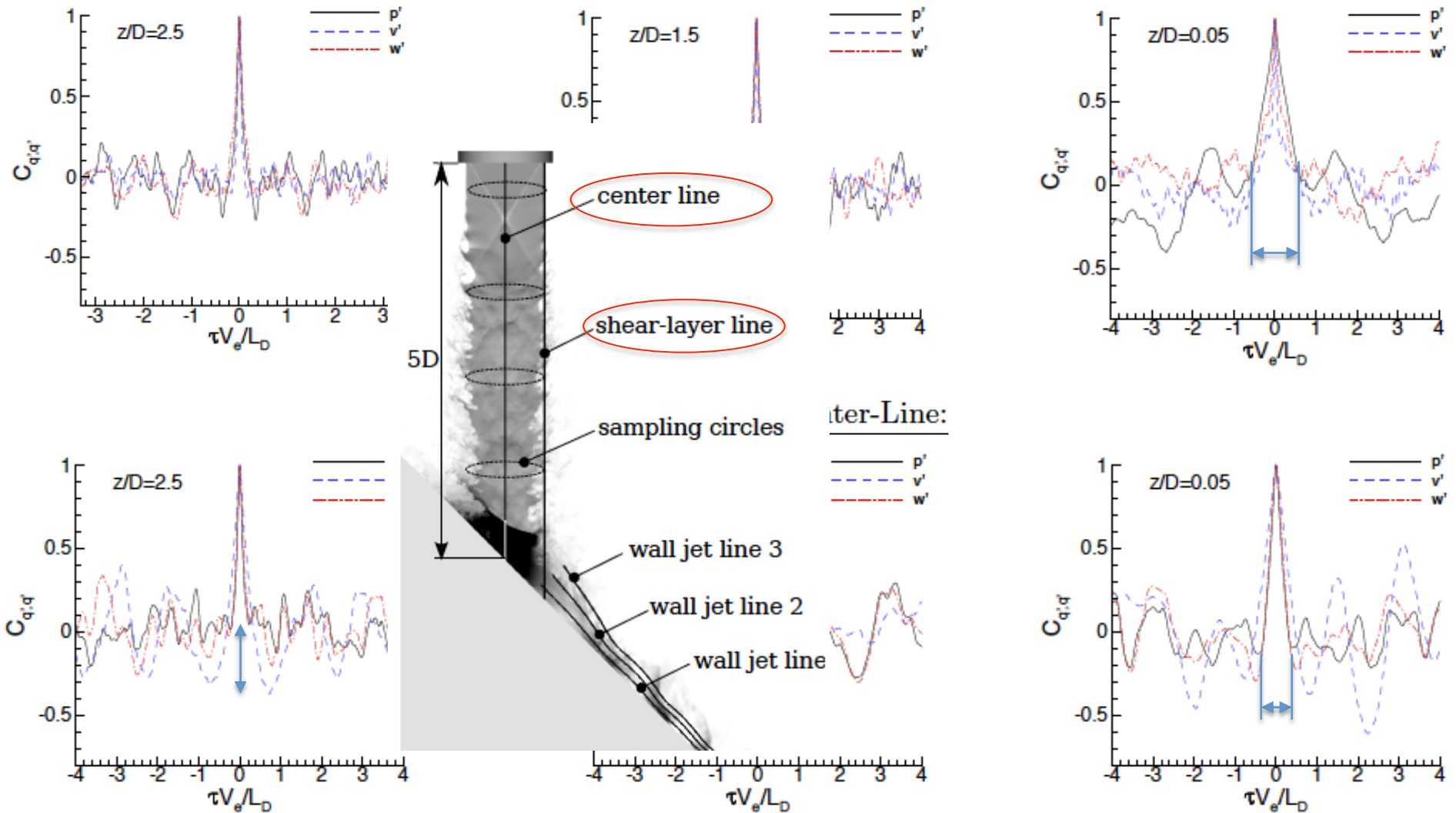
Interaction zone

- Significant changes in relevant physical scales
- Distinct differences between pressure and velocity auto-correlations

CENTER LINE VS. SHEAR LAYER



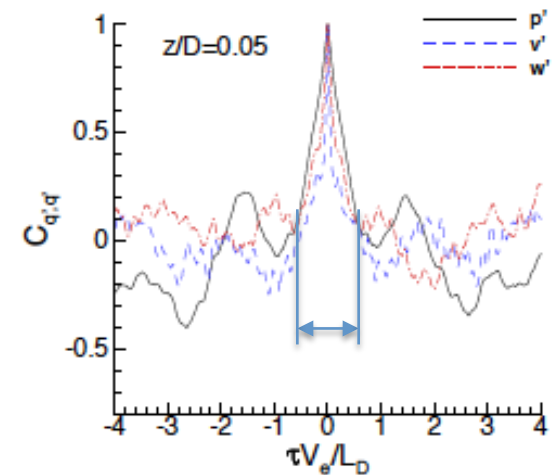
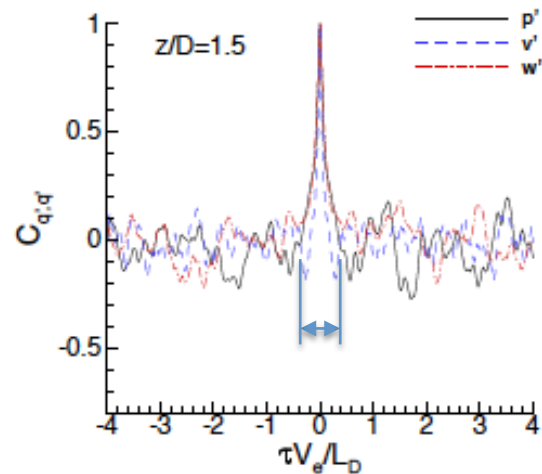
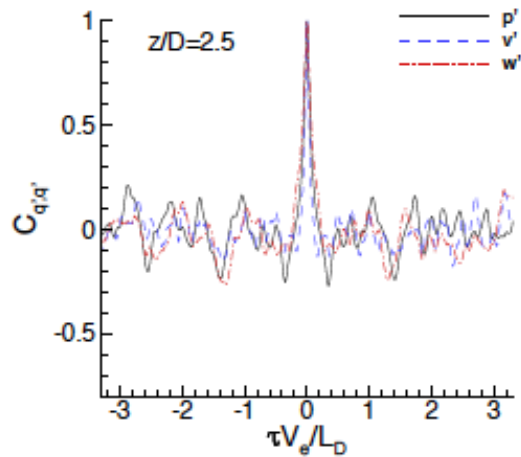
Sample Points on Shear-Layer Line:



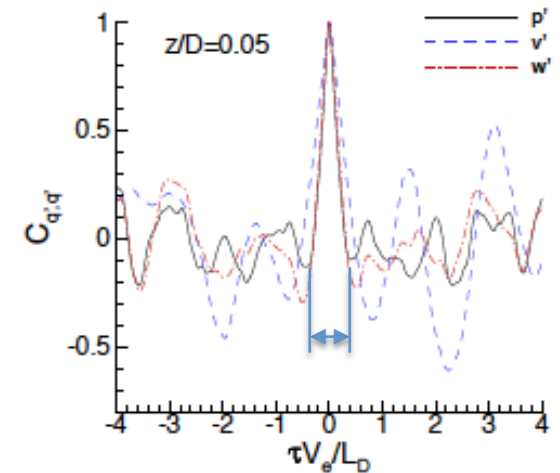
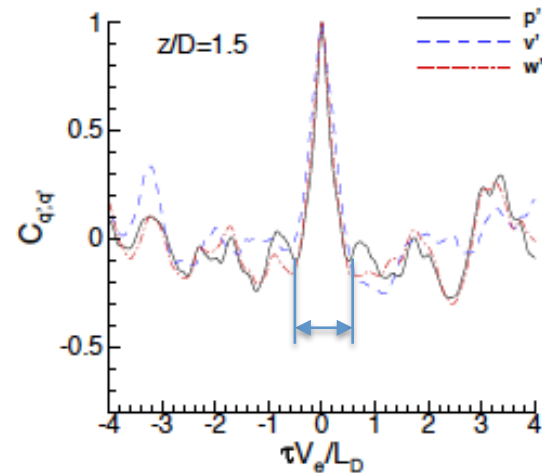
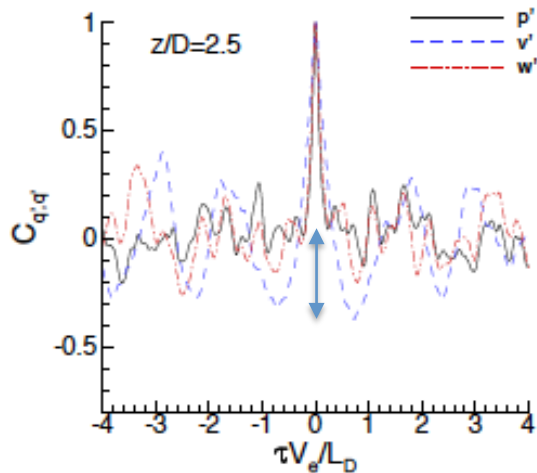
CENTER LINE VS. SHEAR LAYER



Sample Points on Shear-Layer Line:



Sample Points on Center-Line:

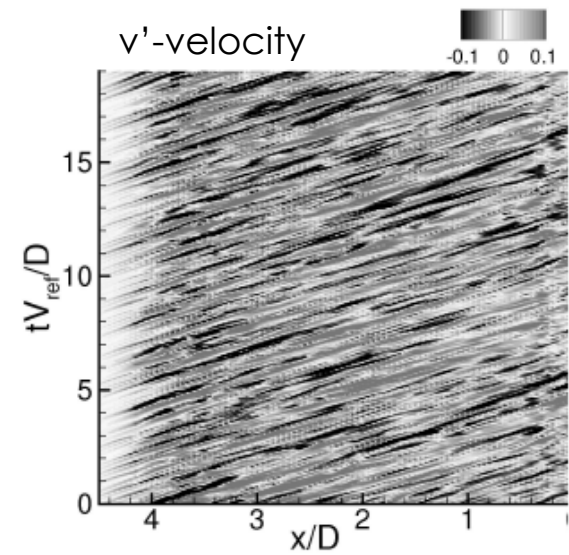
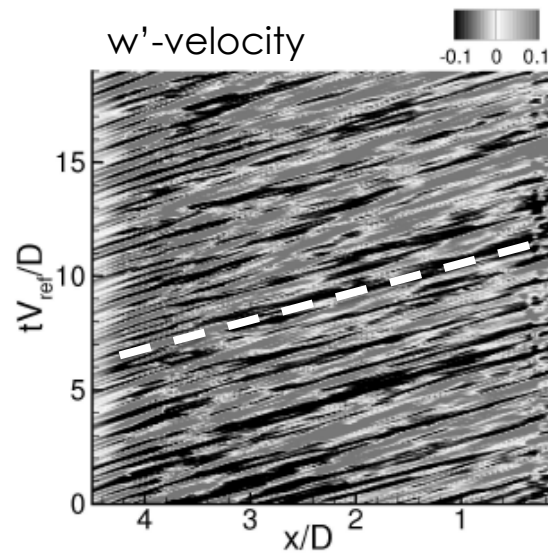
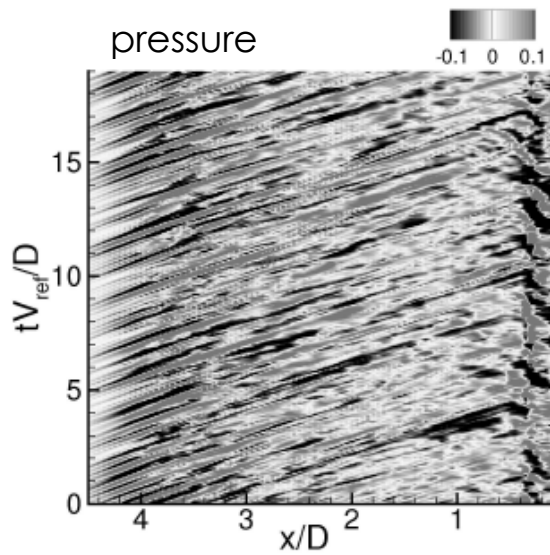


- Turbulence does not enter center of jet before impingement
- Opposite trends in auto-correlations for shear-layer and jet axis

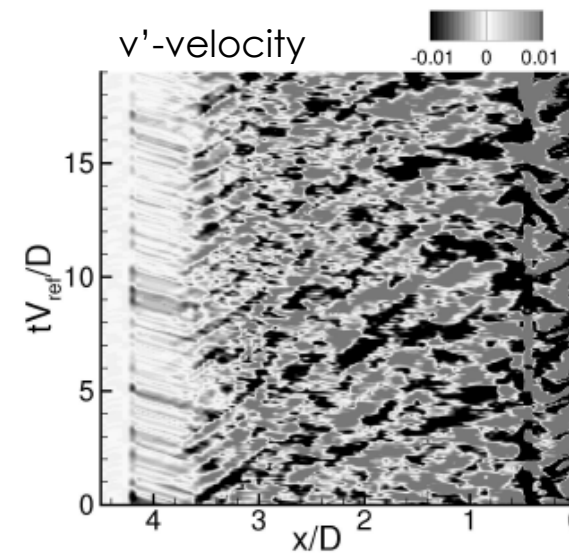
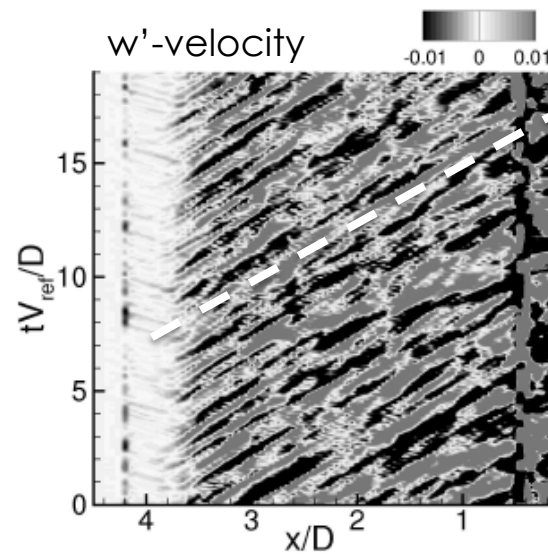
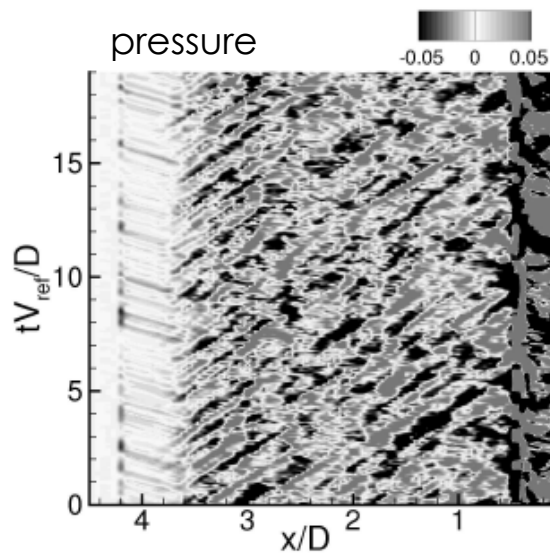
SHEAR LAYER VERSUS JET AXIS



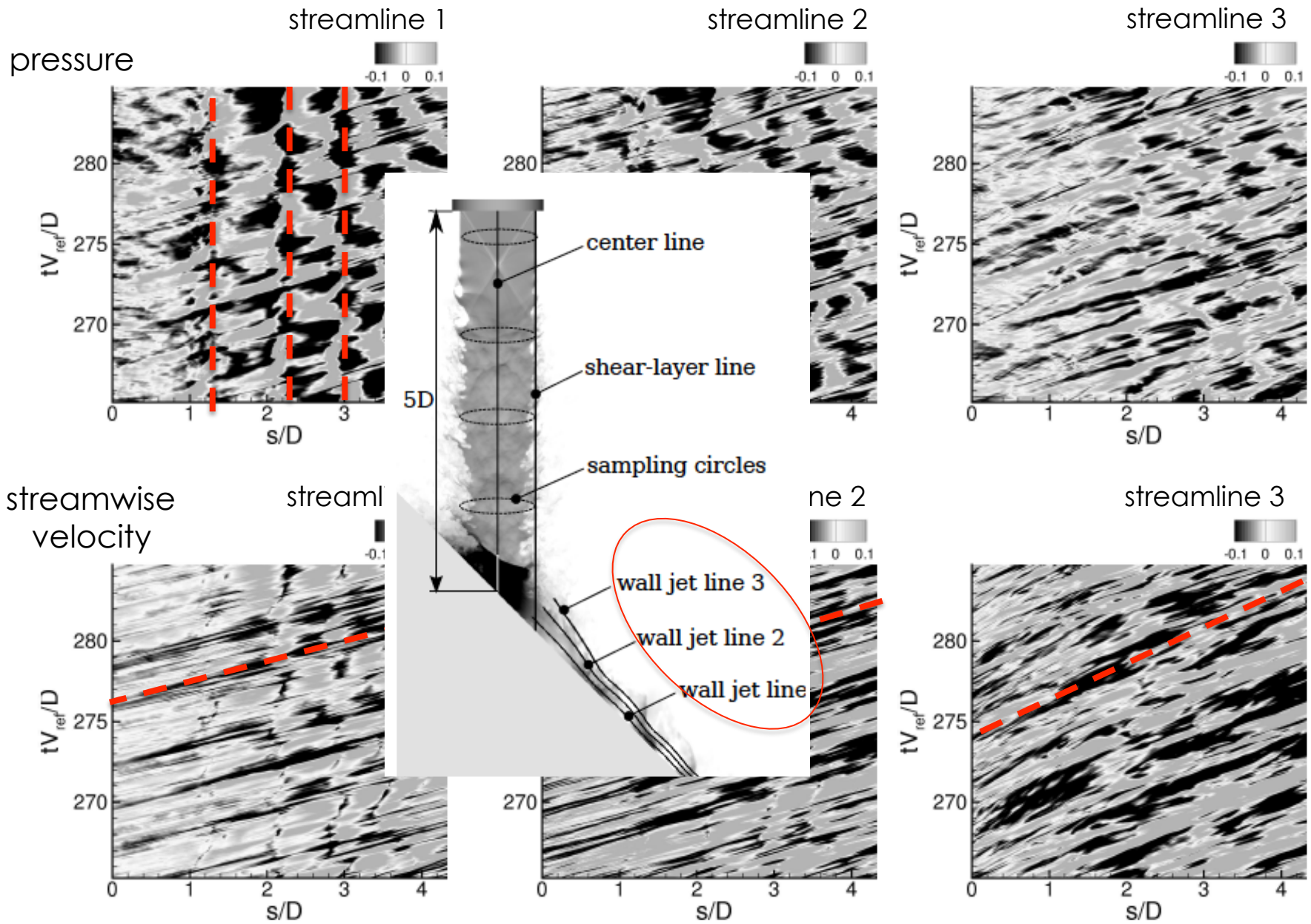
shear-layer



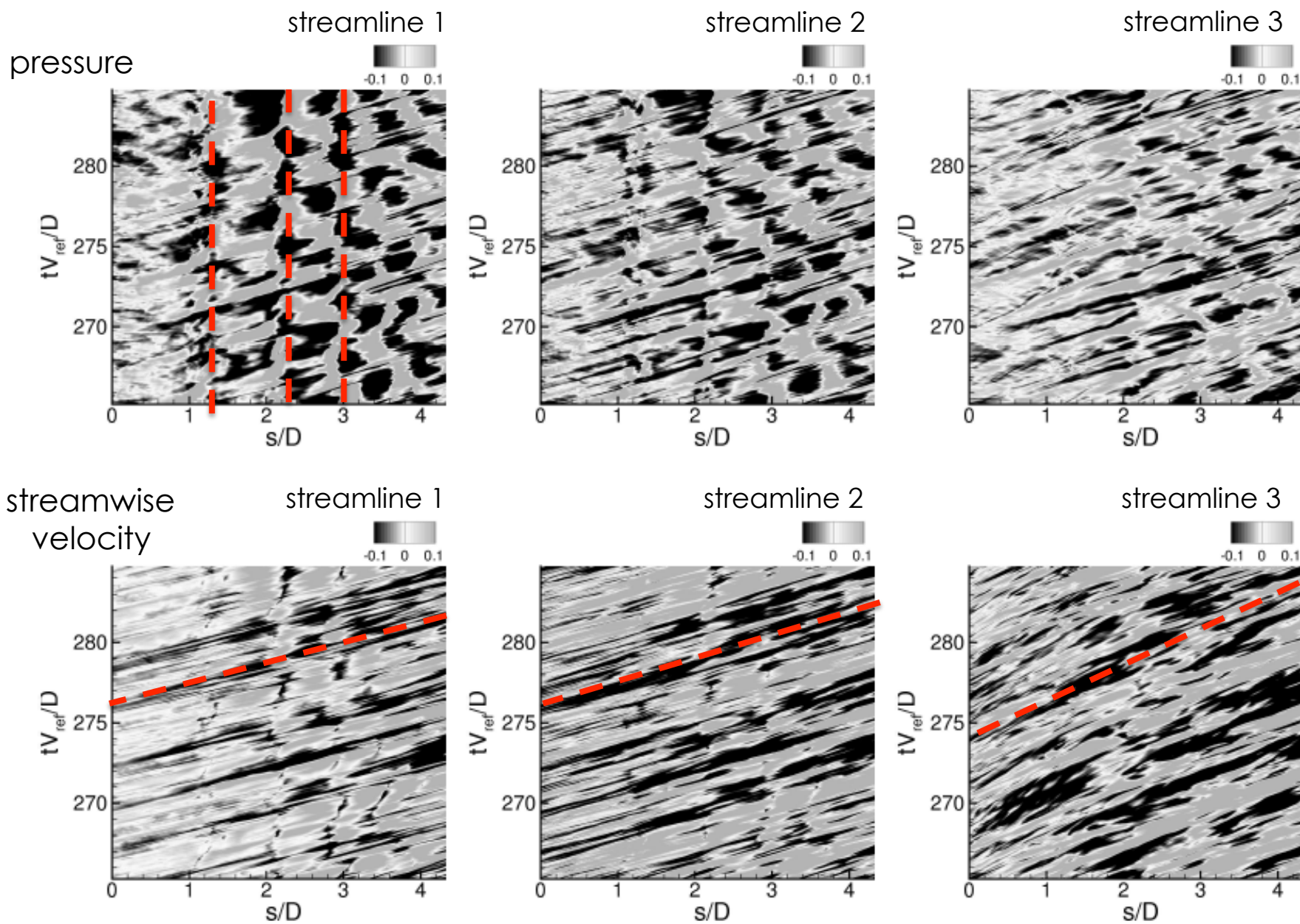
jet axis



SPACE-TIME PLOTS



SPACE-TIME PLOTS

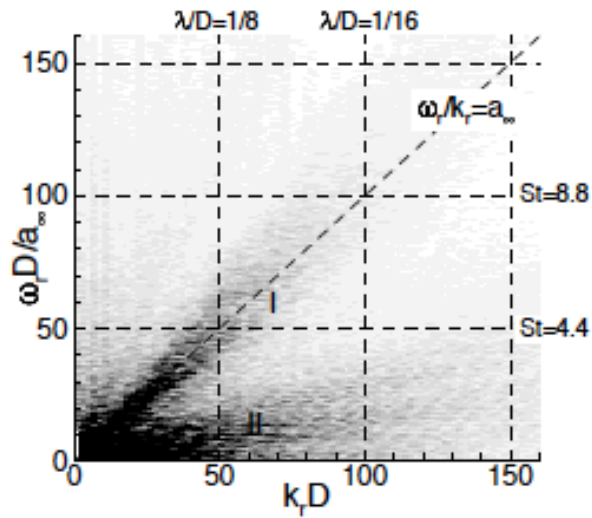


FREQUENCY-WAVENUMBER PLOTS

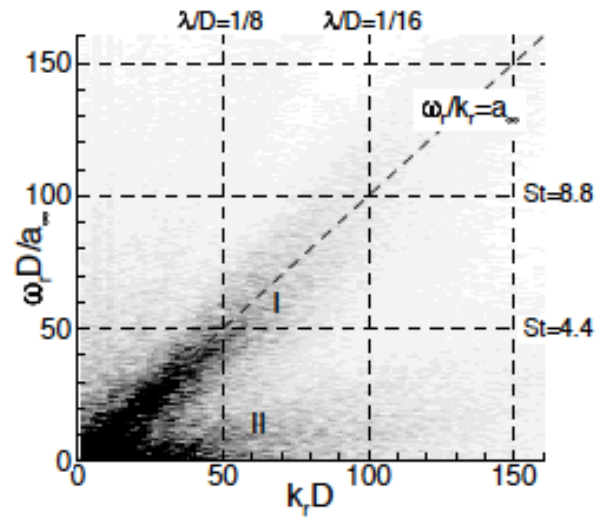


pressure

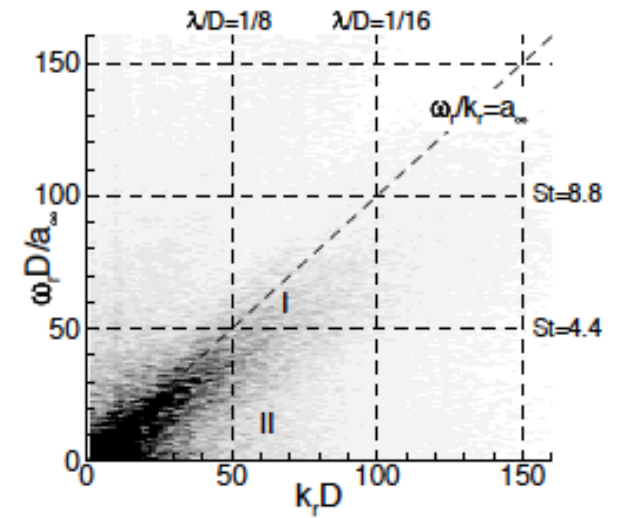
streamline 1



streamline 2

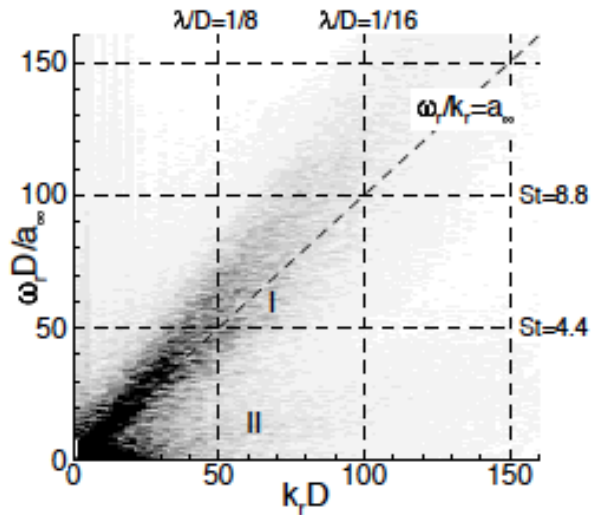


streamline 3

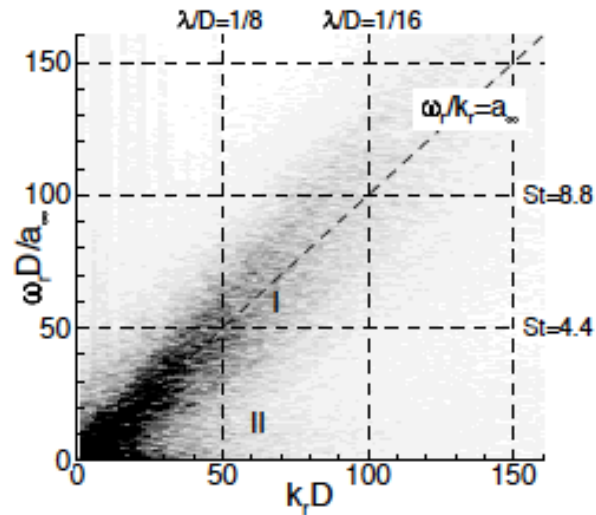


streamwise
velocity

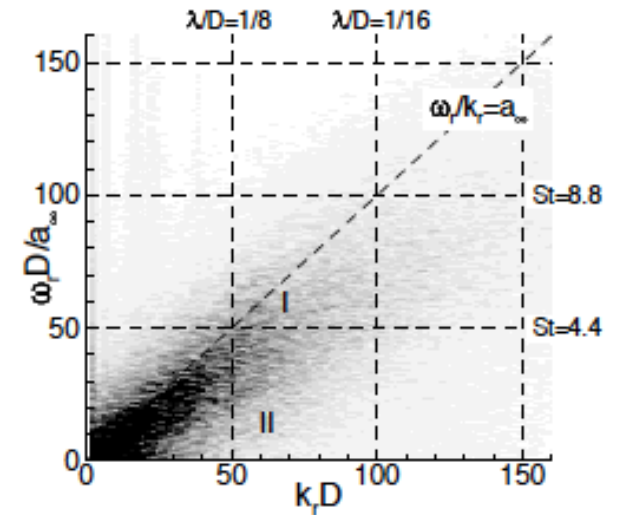
streamline 1



streamline 2



streamline 3

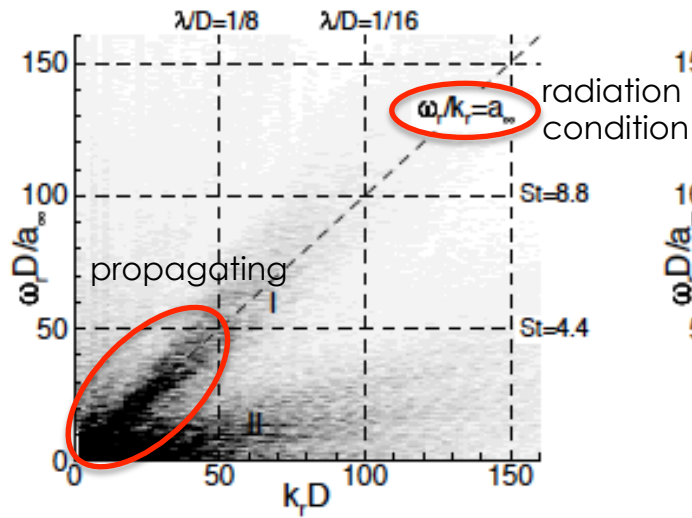


FREQUENCY-WAVENUMBER PLOTS

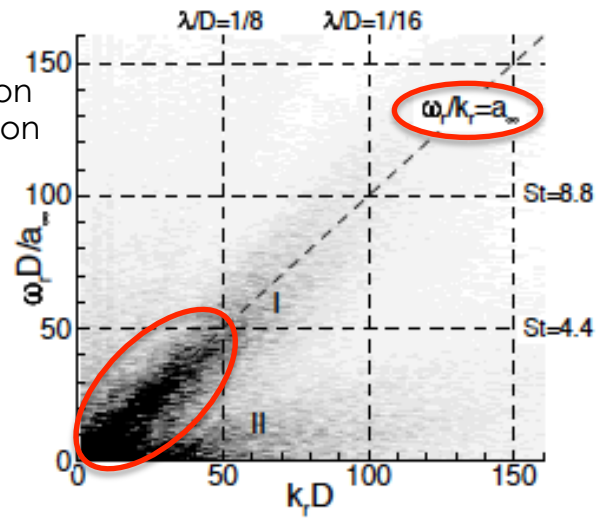


pressure

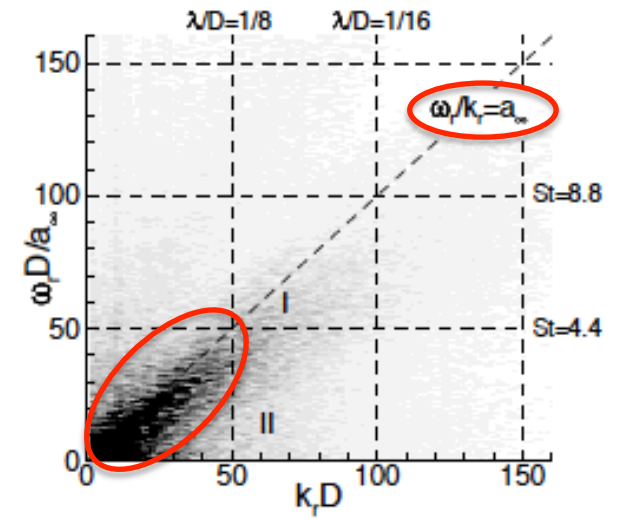
streamline 1



streamline 2

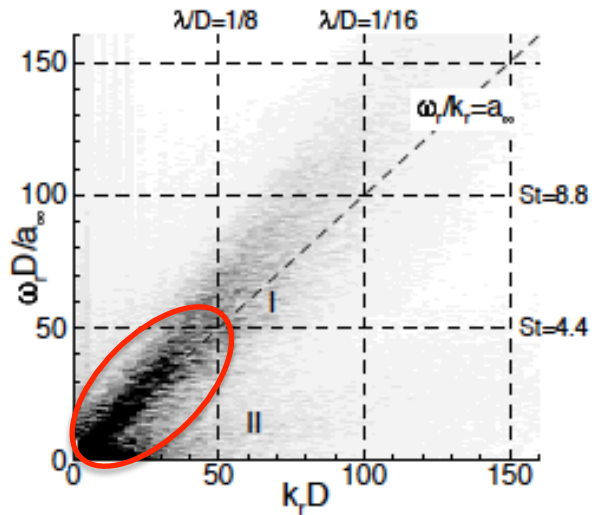


streamline 3

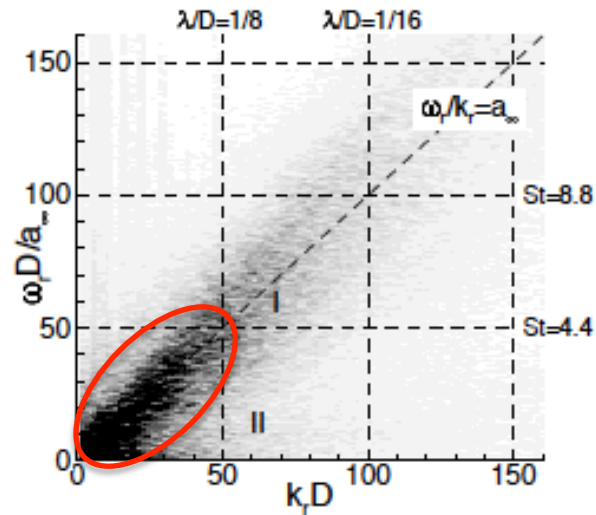


streamwise
velocity

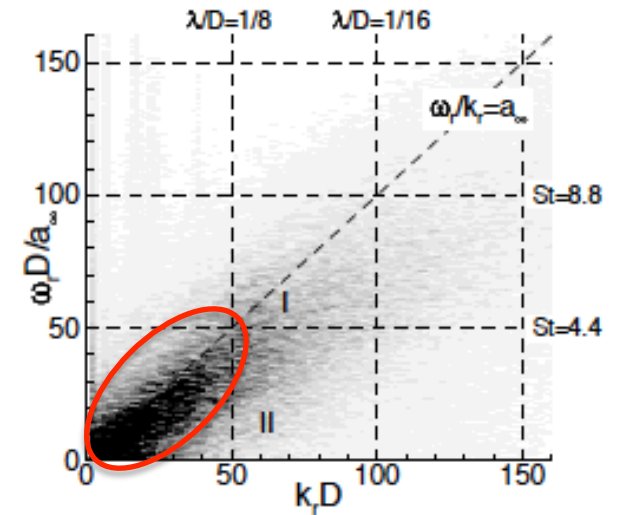
streamline 1



streamline 2



streamline 3

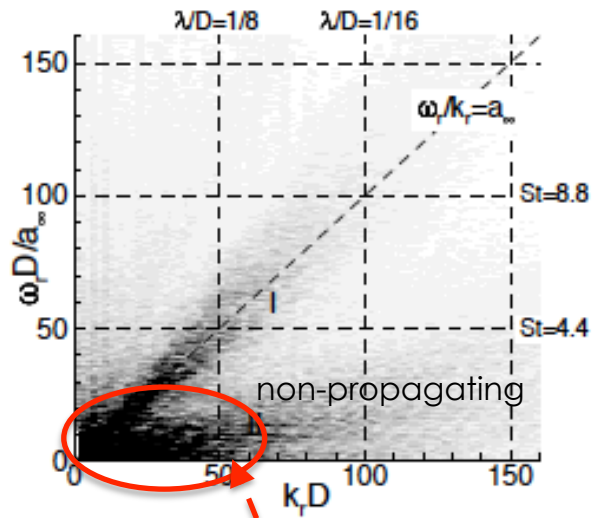


FREQUENCY-WAVENUMBER PLOTS

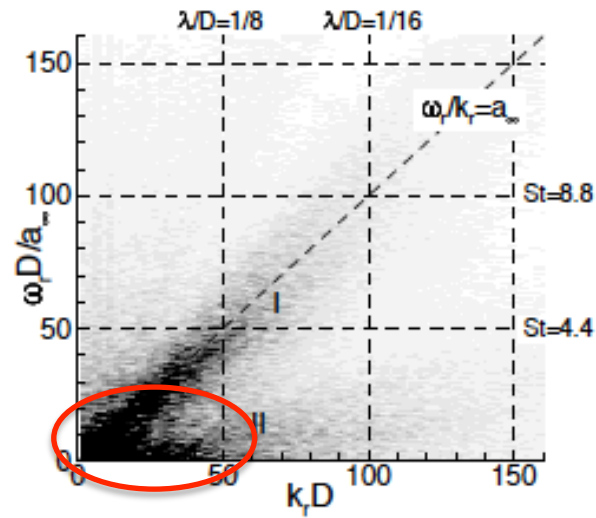


pressure

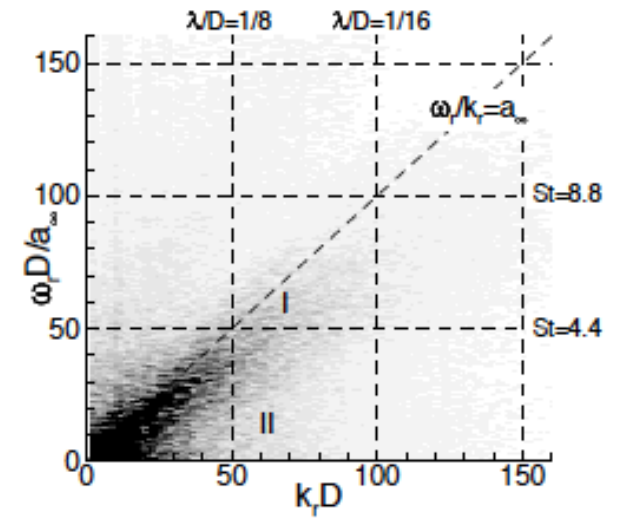
streamline 1



streamline 2

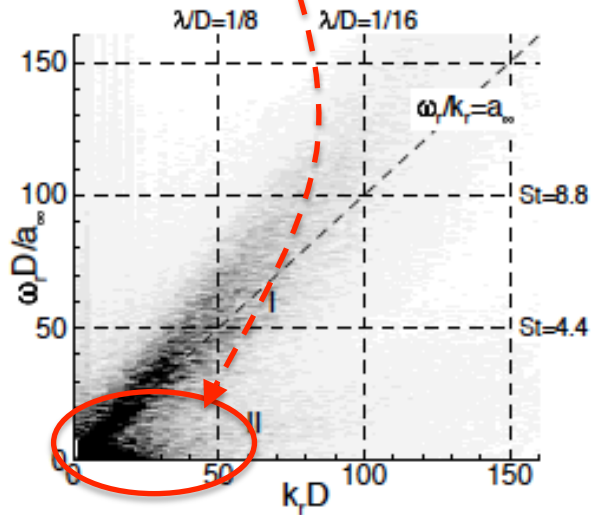


streamline 3

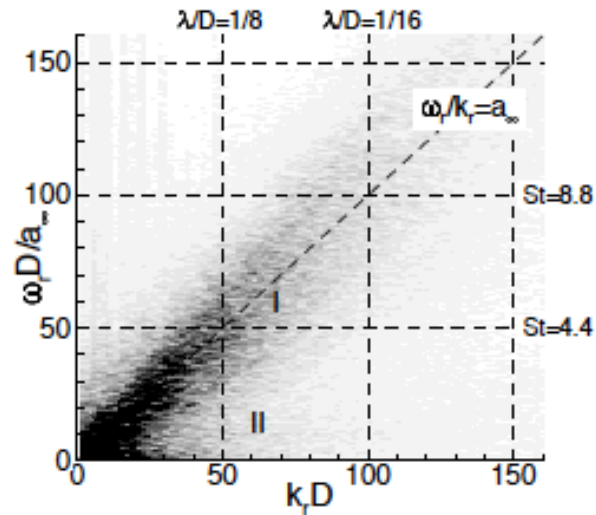


streamwise velocity

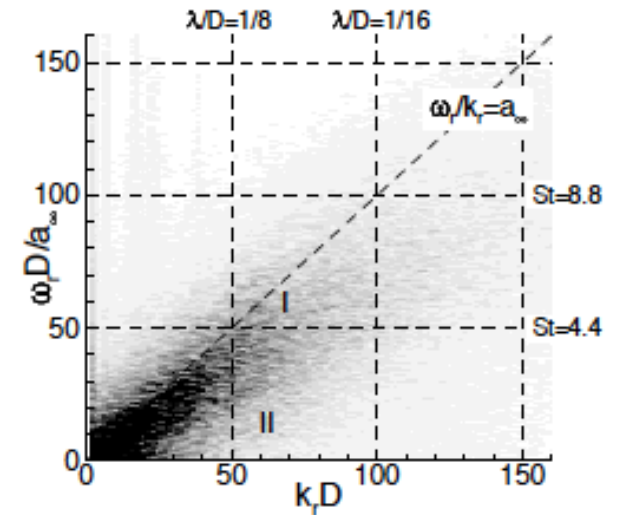
streamline 1



streamline 2



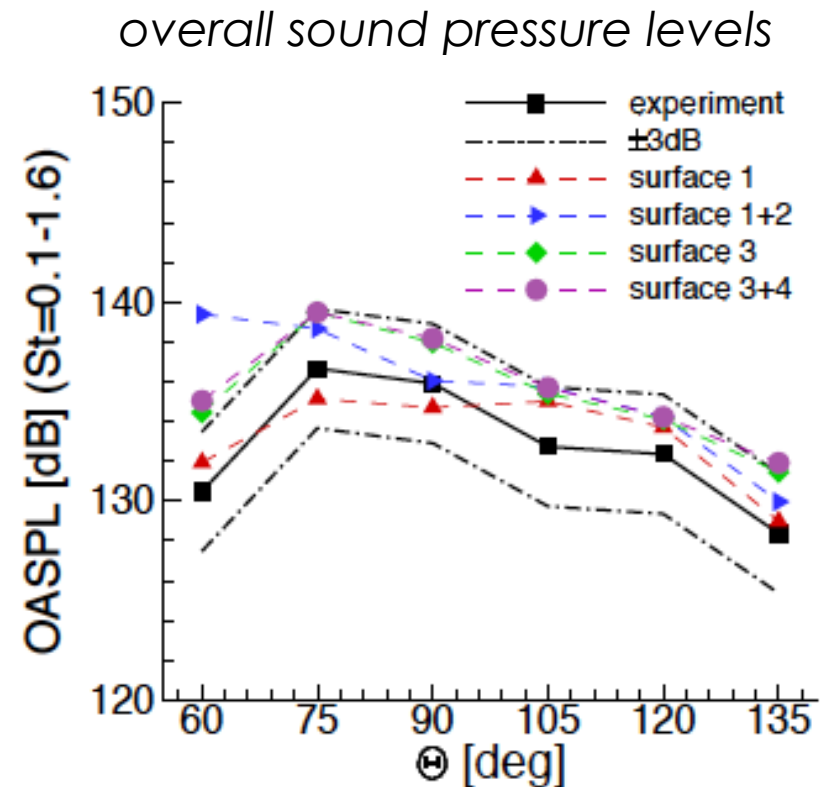
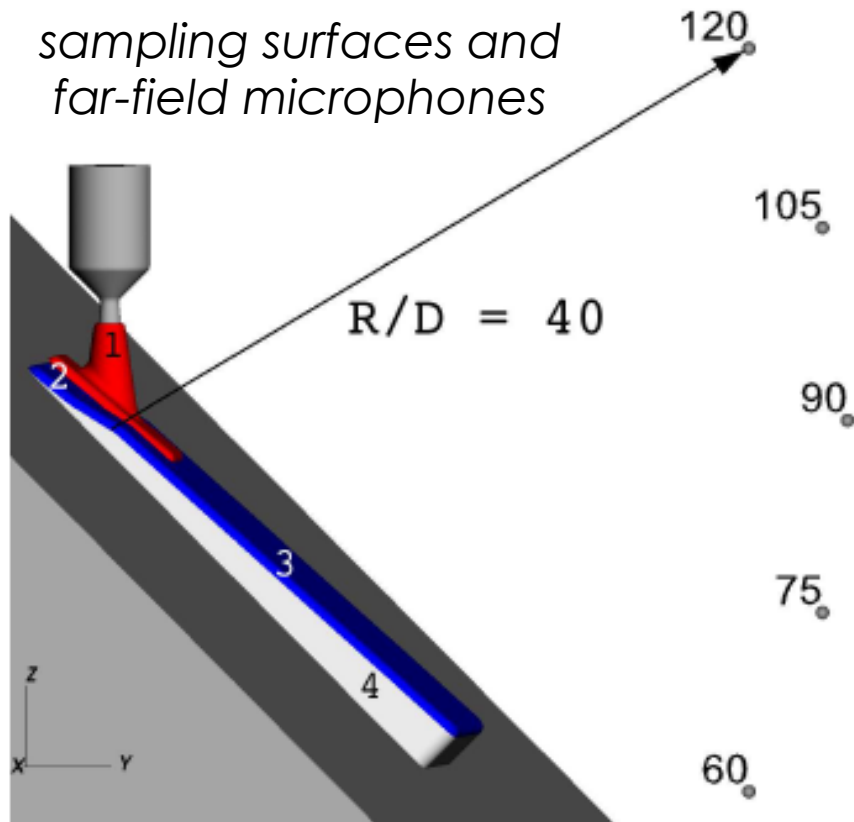
streamline 3





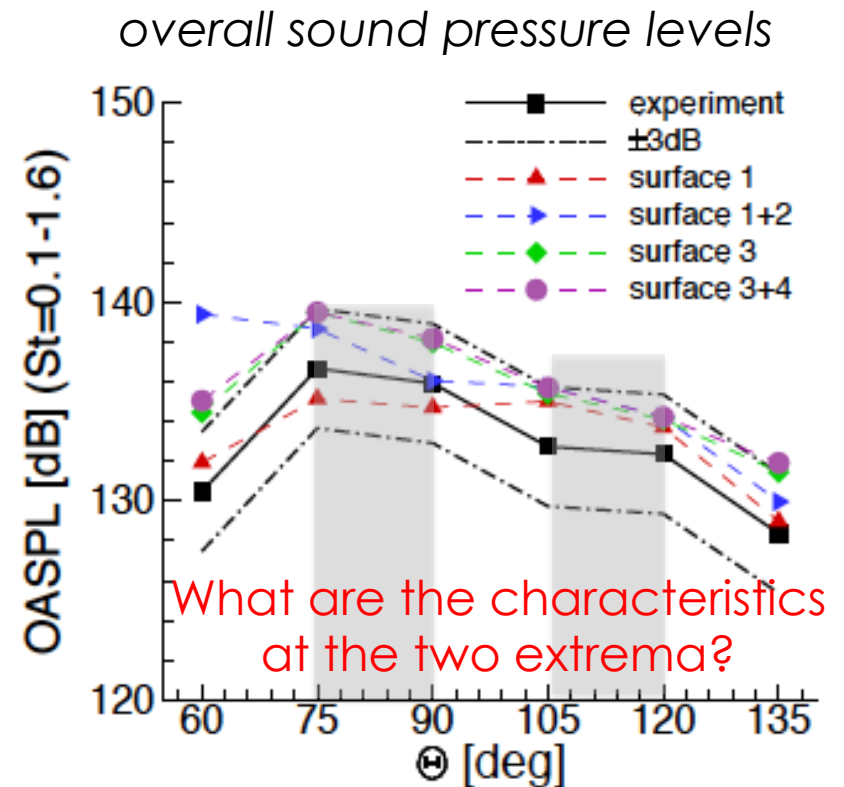
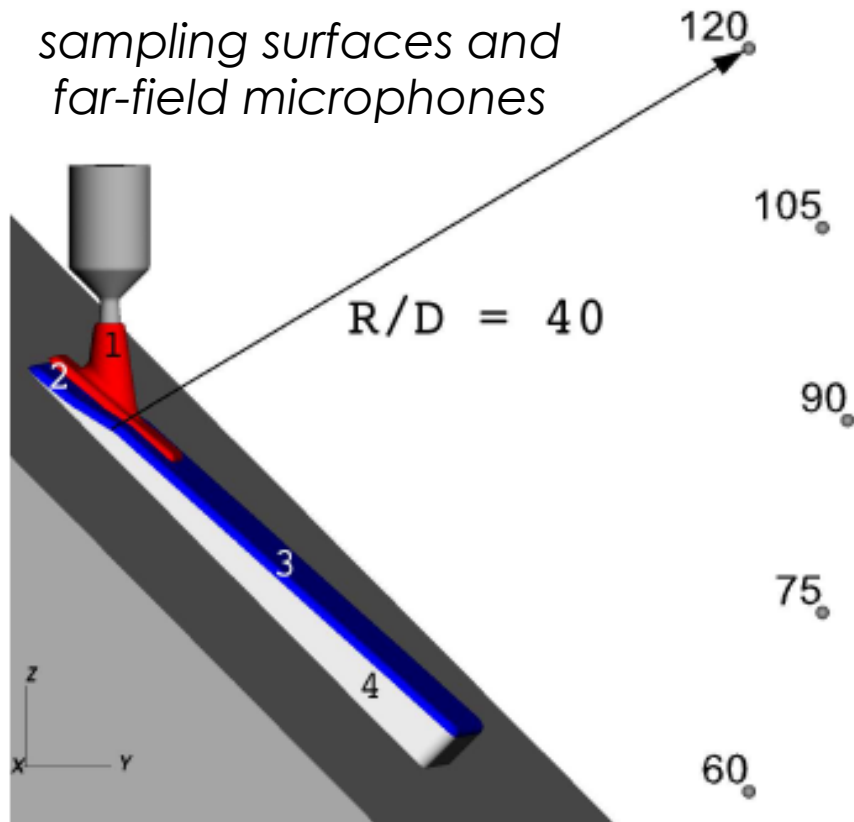
- Introduction to jet noise source identification and characterization
- Computational Simulation Strategy
- Characterization of Flow Field in Source Region
- **Acoustic Wave Propagation Pattern**
- Noise Source Identification
 - Causality Method
 - Proper Orthogonal Decomposition
- Discussion

ACOUSTIC WAVE PROPAGATION PATTERN



- Comparison with experiments by Akamine *et al.* (2014)
- Applied different sampling surfaces with FWH solver
- No-scattering effects observed
- Experiments matched within ± 3 dB
- Two peaks in OASPL far-field spectra at $\Theta \approx 75^\circ$ and $\Theta \approx 120^\circ$

ACOUSTIC WAVE PROPAGATION PATTERN

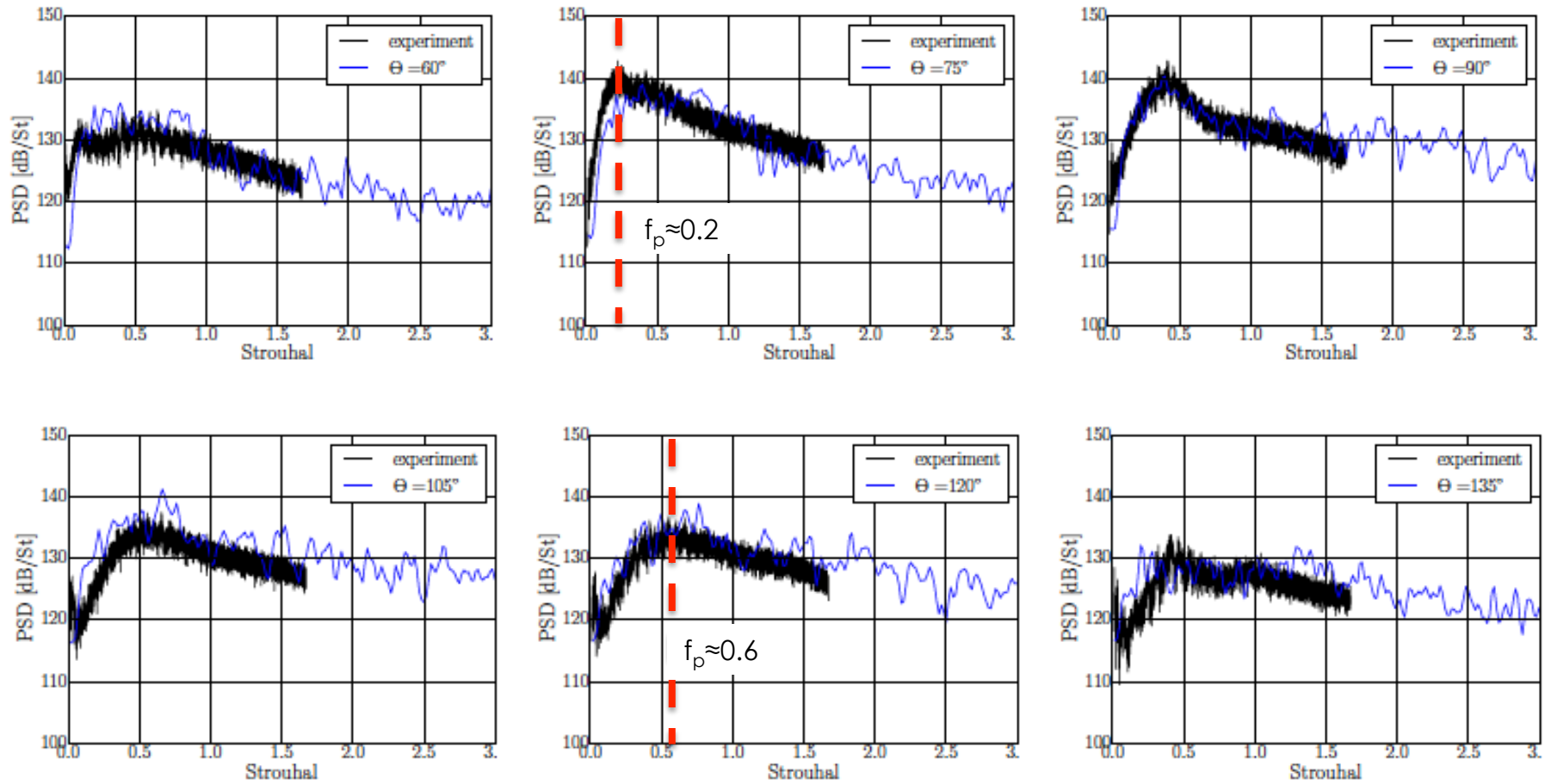


- Comparison with experiments by Akamine *et al.* (2014)
- Applied different sampling surfaces with FWH solver
- No-scattering effects observed
- Experiments matched within $\pm 3dB$
- Two peaks in OASPL far-field spectra at $\Theta \approx 75^\circ$ and $\Theta \approx 120^\circ$

COMPARISON WITH EXPERIMENTS



Power Spectral Density at different field probes

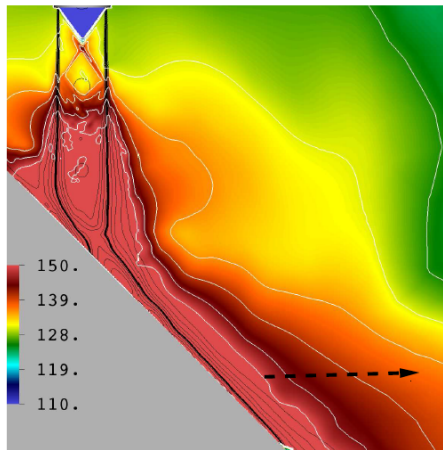


- Close match with experiments
 - Widely different peak frequencies for $\Theta=75^\circ$ and $\Theta=120^\circ$
- Indicates that the noise generation mechanisms are different

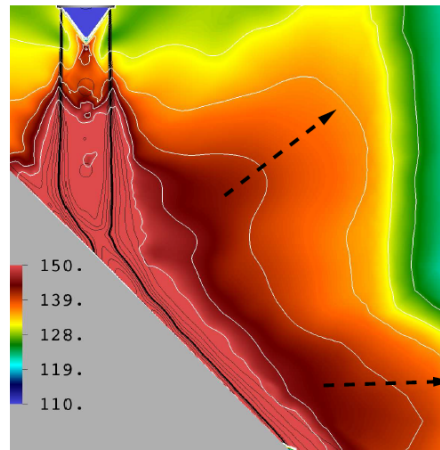
NEAR-FIELD SOUND PRESSURE LEVELS



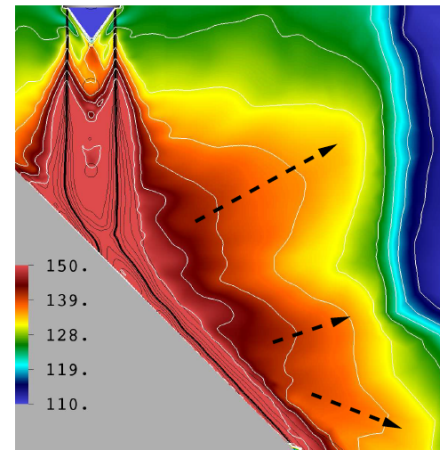
$St=0.16$



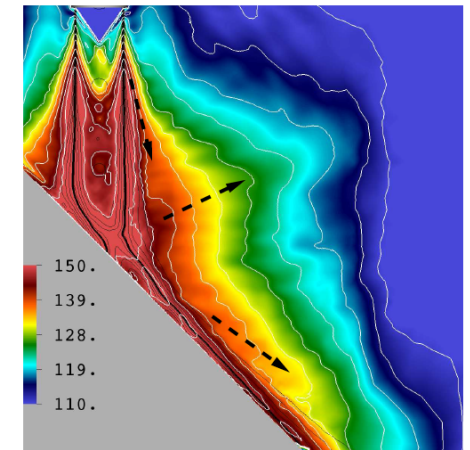
$St=0.33$



$St=0.66$



$St=1.31$



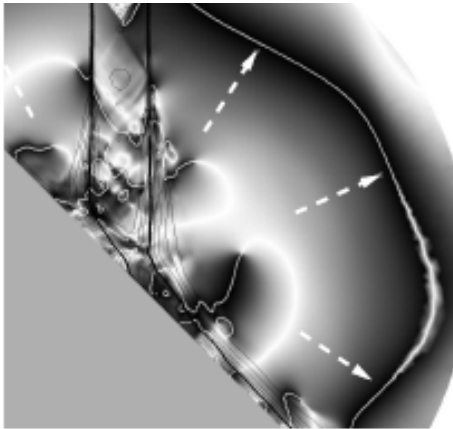
octave-banded SPL (in db)

- It is highly unlikely that distinct noise sources have similar directional dependence
- SPL contours do not provide information about propagation direction
- Three noise generation regions can be observed
 - (1) Shear-layer, (2) impingement region, & (3) wall jet
- For $St=0.16$, wall jet is most dominant noise contributor
- Small SPL for noise generated in impingement region with $St=0.16$

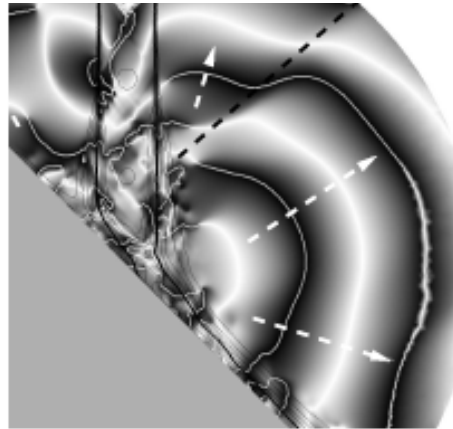
NEAR-FIELD WAVE PROPAGATION PATTERN



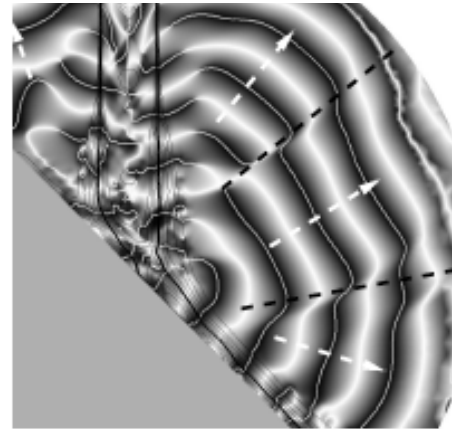
$St_0=0.16$



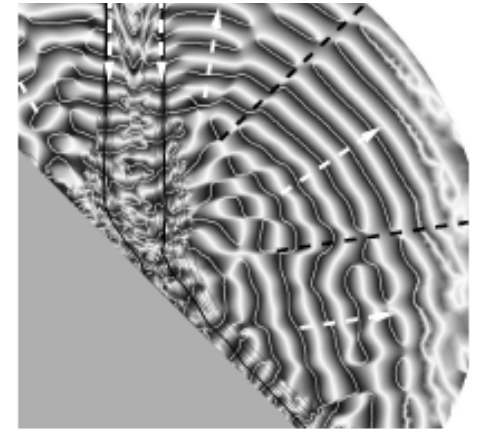
$St_0=0.33$



$St_0=0.66$



$St_0=1.31$



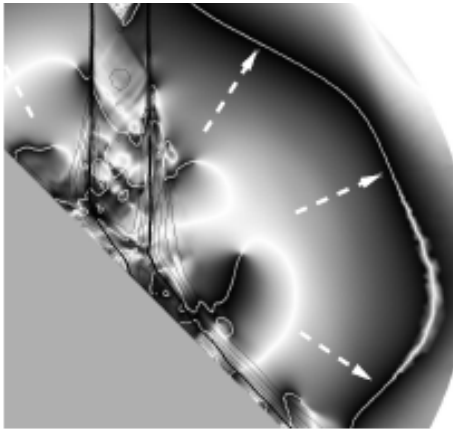
phase ($-\pi \leq \phi < \pi$) at center frequency (St_0)

- Phase plots do not provide information about amplitude information
- Different types of waves (not only acoustic) can be visualized
- For low frequencies, contours continuously extend into wall jet
 - Indicates coupling (phase-locked)
- Shock oscillations cannot easily be identified (not a travelling wave)
- Waves fronts from aforementioned noise sources can be seen

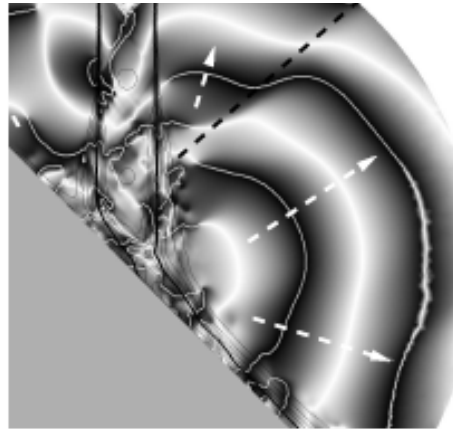
NEAR-FIELD WAVE PROPAGATION PATTERN



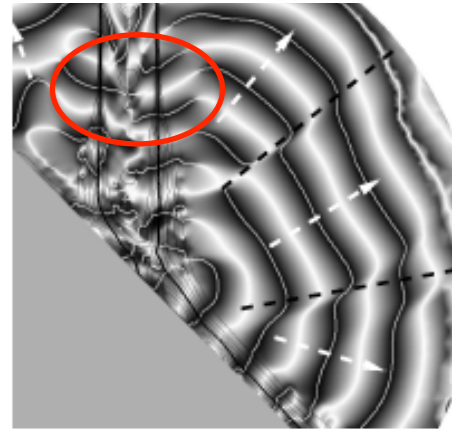
$St_0=0.16$



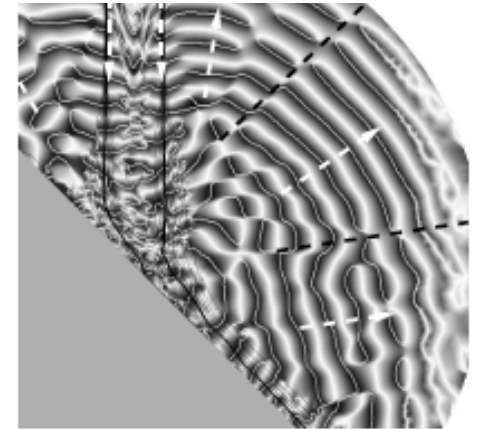
$St_0=0.33$



$St_0=0.66$



$St_0=1.31$



phase ($-\pi \leq \phi < \pi$) at center frequency (St_0)

- Phase plots do not provide information about amplitude information
- Different types of waves (not only acoustic) can be visualized
- For low frequencies, contours continuously extend into wall jet
 - Indicates coupling (phase-locked)
- Shock oscillations cannot easily be identified (not a travelling wave)
- Waves fronts from aforementioned noise sources can be seen



- Introduction to jet noise source identification and characterization
- Computational Simulation Strategy
- Characterization of Flow Field in Source Region
- Acoustic Wave Propagation Pattern
- **Noise Source Identification**
 - Causality Method
 - Proper Orthogonal Decomposition
- Discussion

CAUSALITY METHOD



- Starting point is Lighthill's equation:

$$\frac{\partial \rho}{\partial t} - a_\infty^2 \nabla^2 \rho = \frac{\partial^2 T_{ij}}{\partial x_i \partial x_j} \quad T_{ij} = \rho u_i u_j + \delta_{ij} (p - a_\infty^2 \rho)$$

(Lighthill's stress tensor)

- Cannot distinguish between radiating and non-radiating solutions
- RHS (Lighthill's stress tensor) is forcing term to wave equation (non-unique)
- Apply free space Green's function and integration by parts:

$$\begin{aligned} \rho'(\mathbf{x}_f, t) &= \int_{t_1}^t \int_V T_{ij}(\mathbf{x}_s, \tau) G(\mathbf{x}_f, t; \mathbf{x}_s, \tau) d\mathbf{x}_s d\tau && \dots \text{volume contribution} \\ &- a_\infty^2 \int_{t_1}^t \int_S \left(\rho'(\mathbf{x}_s, \tau) \frac{\partial G}{\partial y_i} - G \frac{\partial \rho'(\mathbf{x}_s, \tau)}{\partial y_i} \right) n_i ds d\tau && \dots \text{surface contribution} \\ &+ \int_V \left(\rho'(\mathbf{x}_s, \tau) \frac{\partial G}{\partial \tau} - G \frac{\partial \rho'(\mathbf{x}_s, \tau)}{\partial \tau} \right)_{\tau=t_1} d\mathbf{x}_s && \dots \text{initial condition} \end{aligned}$$

- Partial integration (2x) and using symmetry of Green's function

$$\rho'(\mathbf{x}_f, t) = \frac{1}{4\pi a_\infty^2} \frac{\partial^2}{\partial x_i \partial x_j} \int_V \frac{T_{ij}(\mathbf{x}_s, t')}{|\mathbf{x}_f - \mathbf{x}_s|} dV, \dots t' = t - \tau_1 \text{ (retarded time),}$$

xf: field point, xs: source point

CAUSALITY METHOD



- Starting point is Lighthill's equation:

$$\frac{\partial \rho}{\partial t} - a_\infty^2 \nabla^2 \rho = \frac{\partial^2 T_{ij}}{\partial x_i \partial x_j} \quad T_{ij} = \rho u_i u_j + \delta_{ij} (p - a_\infty^2 \rho)$$

(Lighthill's stress tensor)

- Cannot distinguish between radiating and non-radiating solutions
- RHS (Lighthill's stress tensor) is forcing term to wave equation (non-unique)
- Apply free space Green's function and integration by parts:

$$\begin{aligned} \rho'(\mathbf{x}_f, t) &= \int_{t_1}^t \int_V T_{ij}(\mathbf{x}_s, \tau) G(\mathbf{x}_f, t; \mathbf{x}_s, \tau) d\mathbf{x}_s d\tau && \dots \text{volume contribution} \\ &- a_\infty^2 \int_{t_1}^t \int_S \left(\rho'(\mathbf{x}_s, \tau) \frac{\partial G}{\partial y_i} - G \frac{\partial \rho'(\mathbf{x}_s, \tau)}{\partial y_i} \right) n_i ds d\tau && \dots \text{surface contribution} \\ &+ \int_V \left(\rho'(\mathbf{x}_s, \tau) \frac{\partial G}{\partial \tau} - G \frac{\partial \rho'(\mathbf{x}_s, \tau)}{\partial \tau} \right)_{\tau=t_1} d\mathbf{x}_s && \dots \text{initial condition} \end{aligned}$$

- Partial integration (2x) and using symmetry of Green's function

$$\rho'(\mathbf{x}_f, t) = \frac{1}{4\pi a_\infty^2} \frac{\partial^2}{\partial x_i \partial x_j} \int_V \frac{T_{ij}(\mathbf{x}_s, t')}{|\mathbf{x}_f - \mathbf{x}_s|} dV, \dots t' = t - \tau_1 \text{ (retarded time),}$$

xf: field point, xs: source point



- Finally, computing acoustic intensity we arrive at:

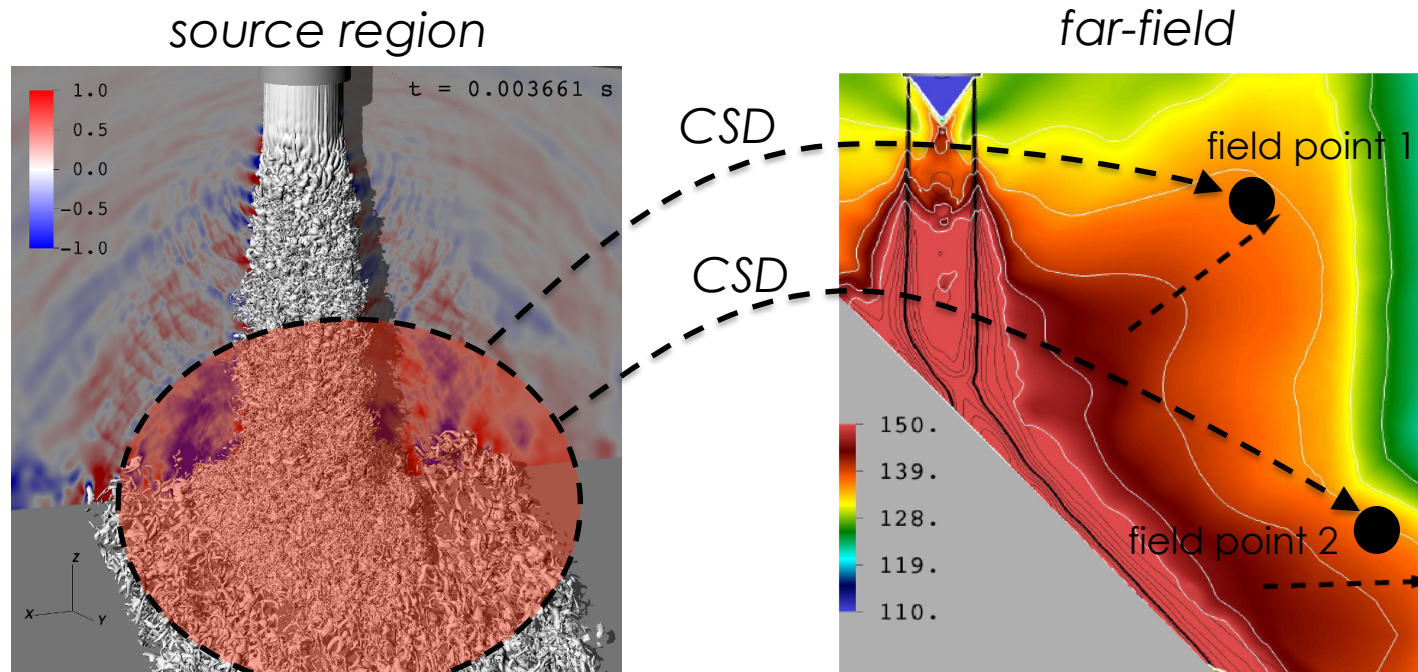
$$\begin{aligned} \langle p', p' \rangle (\mathbf{x}_f, \tau) &= \left\langle \frac{1}{4\pi a_0^2 r} \int_V \frac{\partial^2}{\partial t'^2} T_r(\mathbf{x}_s, t' + \tau) dV, p'(\mathbf{x}_f, t) \right\rangle \\ \text{(acoustic intensity)} &= \frac{1}{4\pi a_0^2 r} \int_V \frac{\partial^2}{\partial \tau^2} R_{T_r, p'}(\mathbf{x}_s, \mathbf{x}_f, \tau) dV, \end{aligned}$$

- Assumed far-field approximation $x_f \gg x_s$ and use stress tensor component T_r in r-direction ($r = x_f - x_s$)
- Fourier transform to avoid numerical differentiation:

$$PSD_{p'}(\mathbf{x}_f, f) = -\frac{\pi f^2}{r a_\infty^2} \int_V CSD_{T_r, p'}(\mathbf{x}_f, \mathbf{x}_s, f) dV.$$

- Decomposition of stress tensor

$$\langle \rho V_r^2; p' \rangle = \underbrace{\langle 2 \langle \rho \rangle \langle V \rangle_r V_r'; p' \rangle + \langle \rho' \langle V_r \rangle^2; p' \rangle}_{\text{first-order terms}} + \underbrace{\langle 2 \langle V_r \rangle \rho' V_r'; p' \rangle + \langle \langle \rho \rangle V_r'^2; p' \rangle + \langle \rho' V_r'^2; p' \rangle}_{\text{higher-order terms}}$$



- Use normalized and un-normalized correlations
- Few studies have considered entropy fluctuation term ($s' = p' - (a_\infty)^2 \rho'$)
- Essential differences to previous works on free jet:
 - (1) Dipole contribution from surface integral
 - (2) Entropy fluctuation term plays important role
 - (3) Differentiate between normalized and un-normalized correlations
- Evaluate CSD in entire (y,z) -plane
- Two field sensors where used in $\Theta = 120^\circ$ and $\Theta = 75^\circ$ directions

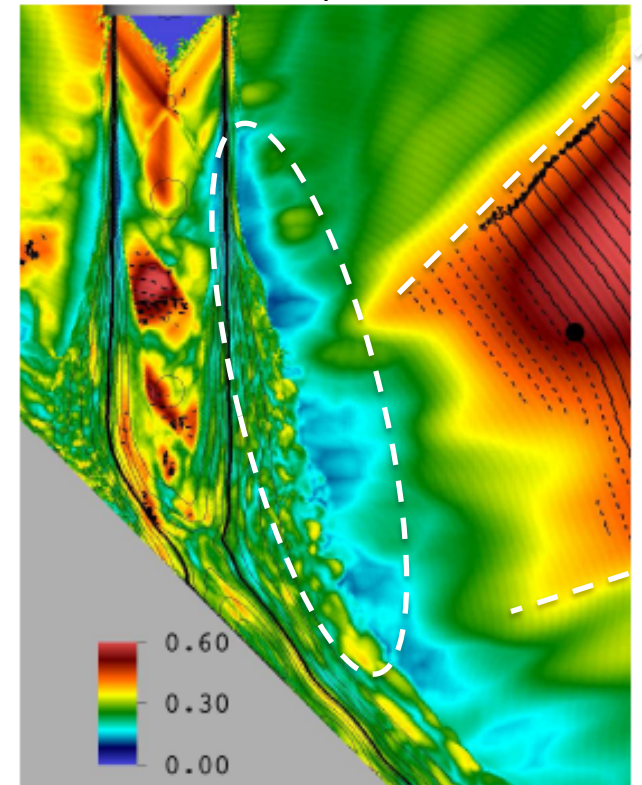
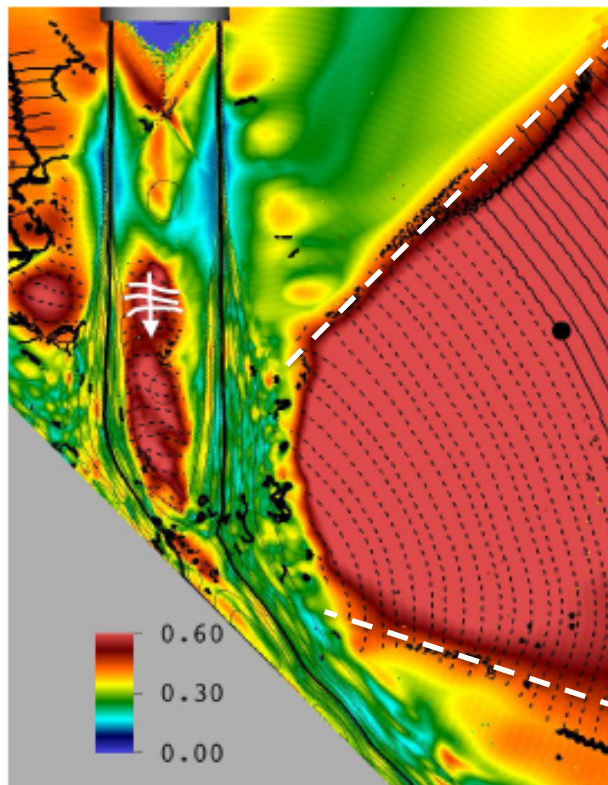
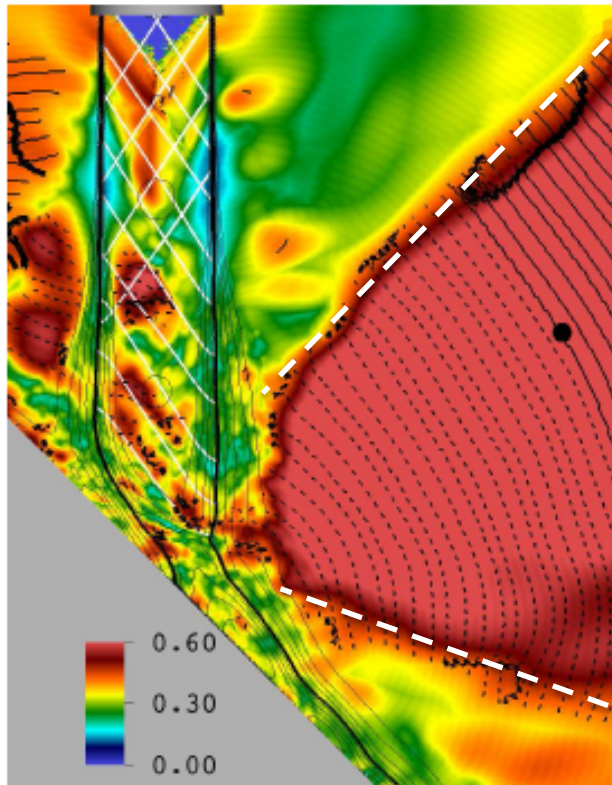
NORMALIZED CROSS-SPECTRAL DENSITY



$$\hat{C}_{p',p'}$$

$$\hat{C}_{p',Vr'}$$

$$\hat{C}_{p',s'}$$



- Note regions with large peak correlation are likely not acoustic source regions
- Wedges define propagation directions
- When backtracking the contour lines into the source region provides approximate source locations
- Since fluctuations are large in the source region signals are strongly randomized (low correlations)

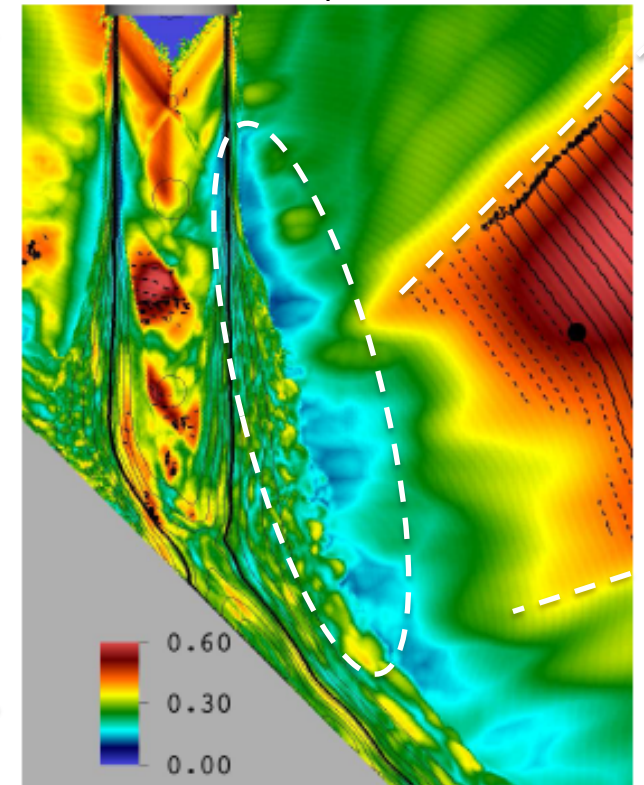
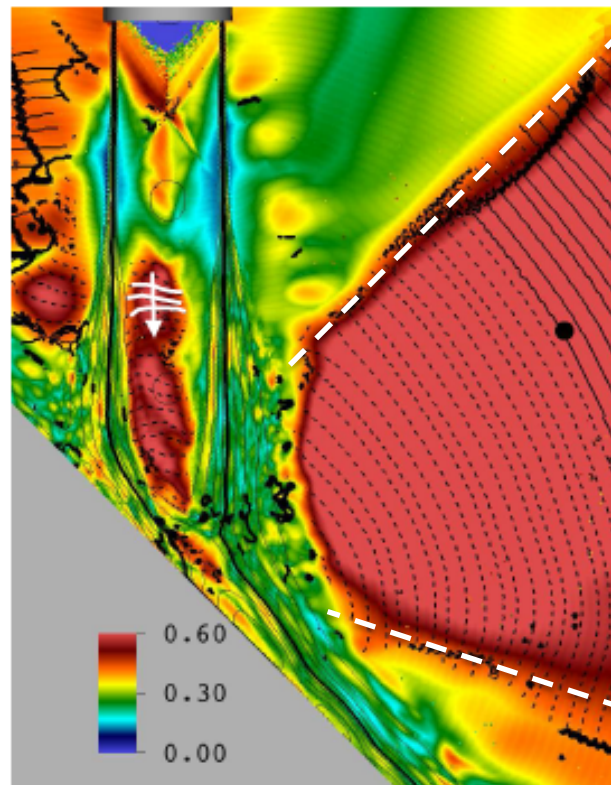
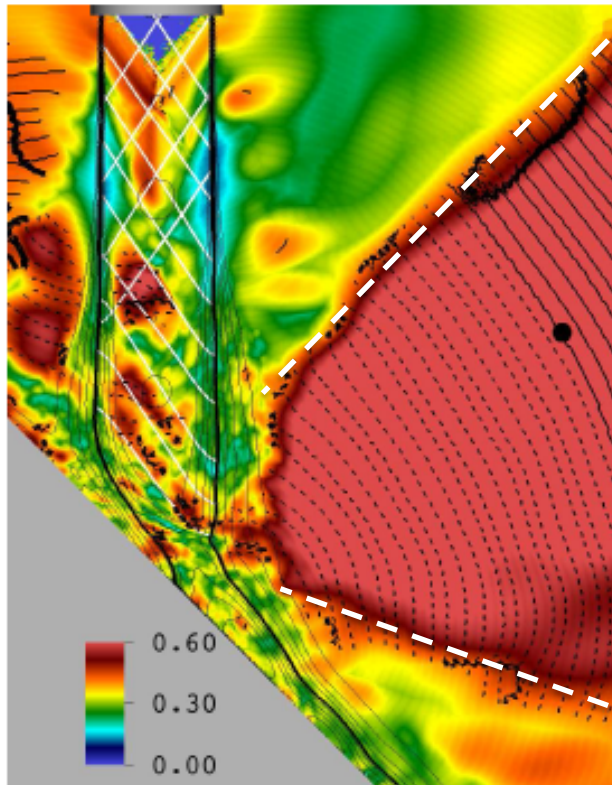
NORMALIZED CROSS-SPECTRAL DENSITY



$$\hat{C}_{p',p'}$$

$$\hat{C}_{p',v_r'}$$

$$\hat{C}_{p',s'}$$



- Large fraction of unsteadiness in the source region is non-radiating
- Dashed contour lines of time delay (dashed $\tau < 0$, solid $\tau > 0$)
- Distance between time delay lines corresponds to speed of sound
- Contribution of cross-spectral density with pressure from surface integral
- Large values of $\hat{C}_{p',v_r'}$ inside jet (coherence length $O(D)$)

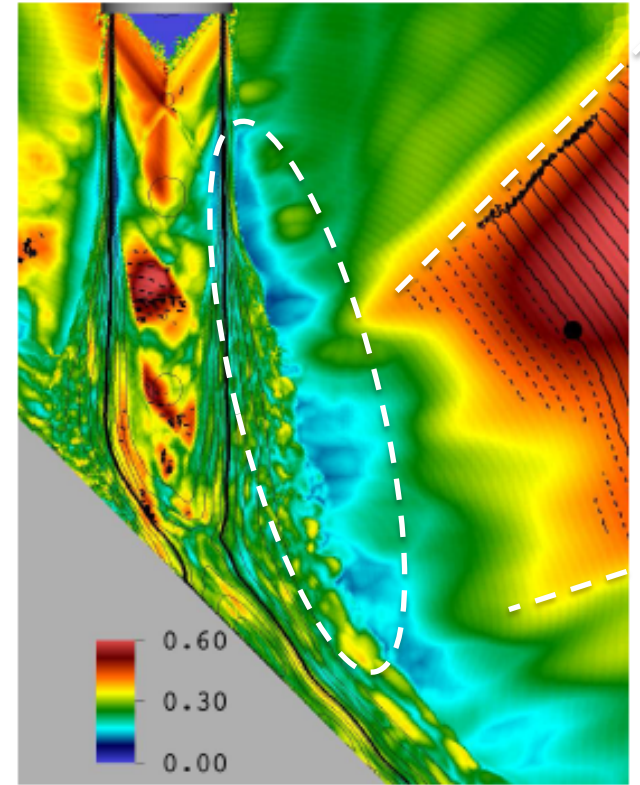
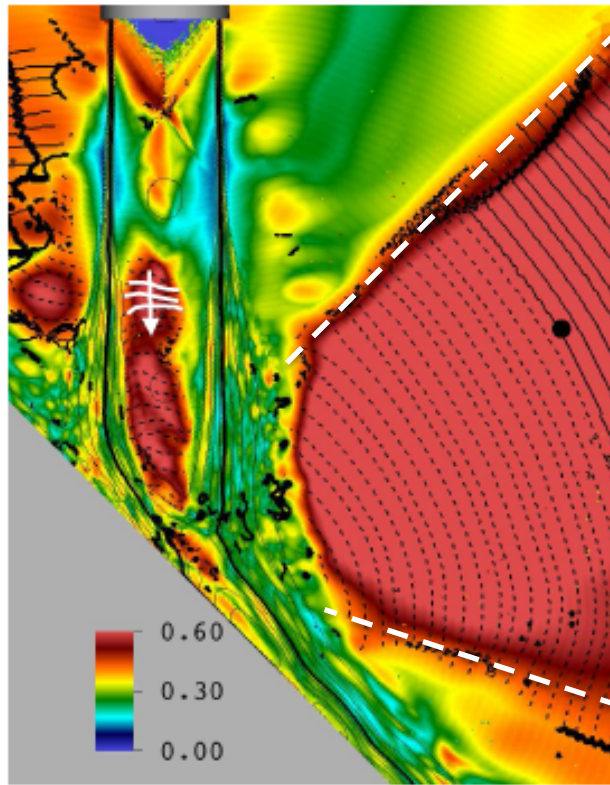
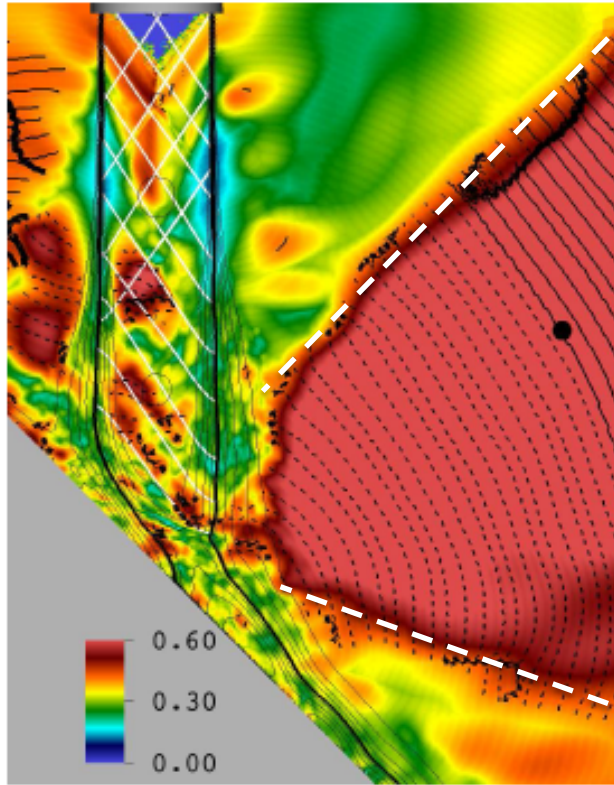
NORMALIZED CROSS-SPECTRAL DENSITY



$$\hat{C}_{p',p'}$$

$$\hat{C}_{p',Vr'}$$

$$\hat{C}_{p',s'}$$

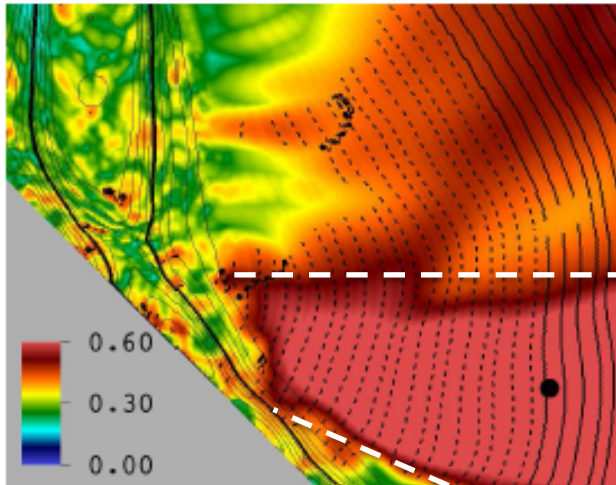


- Flow structures convect with jet flow (sketch added)
- Low $\hat{C}_{p',Vr'}$ in the shear layer (similar to what was observed for free jets)
- Low values of $\hat{C}_{p',s'}$ in shear layer region (not reported before)

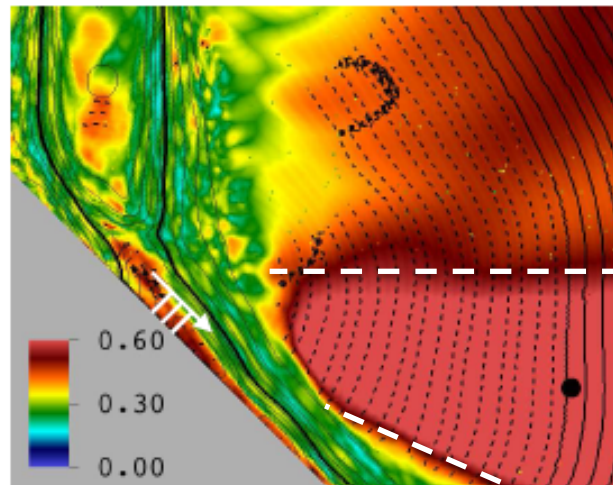
NORMALIZED CROSS-SPECTRAL DENSITY



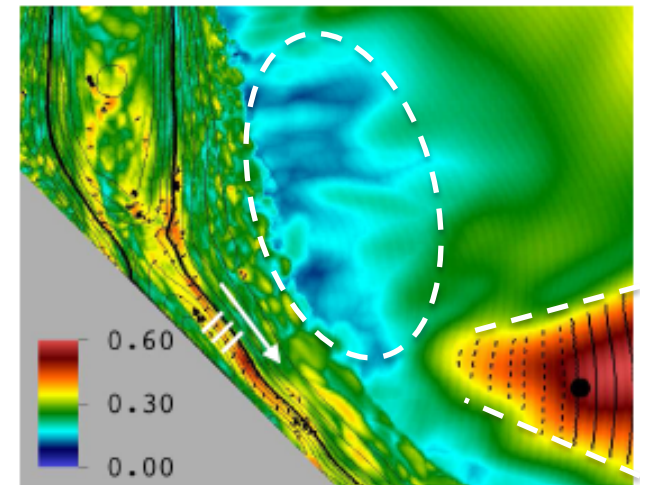
$$\hat{C}_{p',p'}$$



$$\hat{C}_{p',v_r'}$$



$$\hat{C}_{p',s'}$$



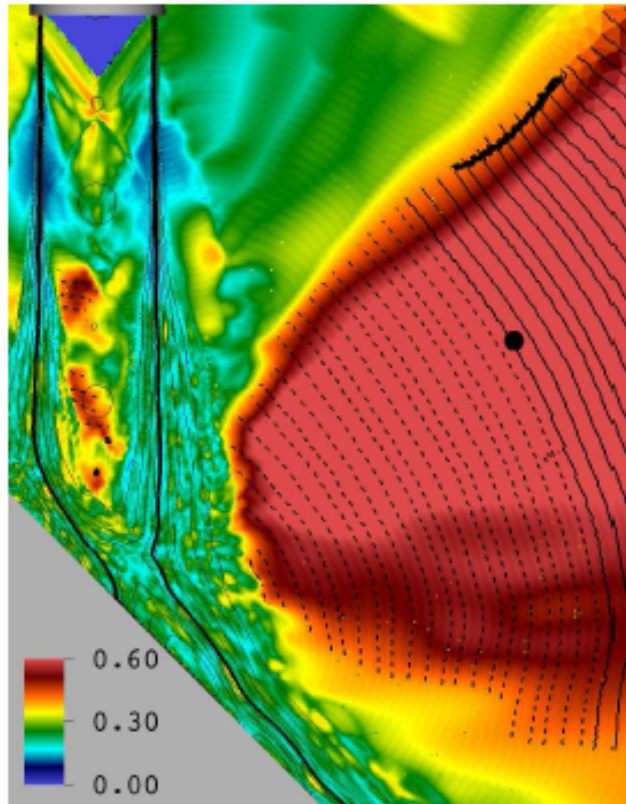
- Two wedges with large $\hat{C}_{p',p'}$ for $\Theta=120^\circ$ and $\Theta=75^\circ$ are separate regions
- Small cross-spectral densities in the jet center
- Large values of $\hat{C}_{p',v_r'}$ in supersonic region of the wall jet (similar to upstream)
- Large values of $\hat{C}_{p',s'}$ at the edge of wall jet's shear layer
- Propagation direction illustrated by sketches
- Meaning of entropy fluctuation term (excess density, $\rho_e = \rho' - \rho' / (a_\infty)^2$)

$$-\frac{\partial^2 \rho_e}{\partial t^2} = \frac{\partial}{\partial t} \left[\underbrace{\left(\frac{a^2}{a_\infty^2} - 1 + \frac{\rho_e}{\rho} \right) \frac{Dp'}{Dt}}_{\text{constant heat capacity}} + \underbrace{\frac{\rho^2}{a_\infty^2} \left(\frac{\partial T}{\partial \rho} \right)_s \frac{Ds}{Dt}}_{\text{non-isentropic process}} + \underbrace{\nabla \cdot (v \rho_e)}_{\text{spatial density variation}} \right]$$

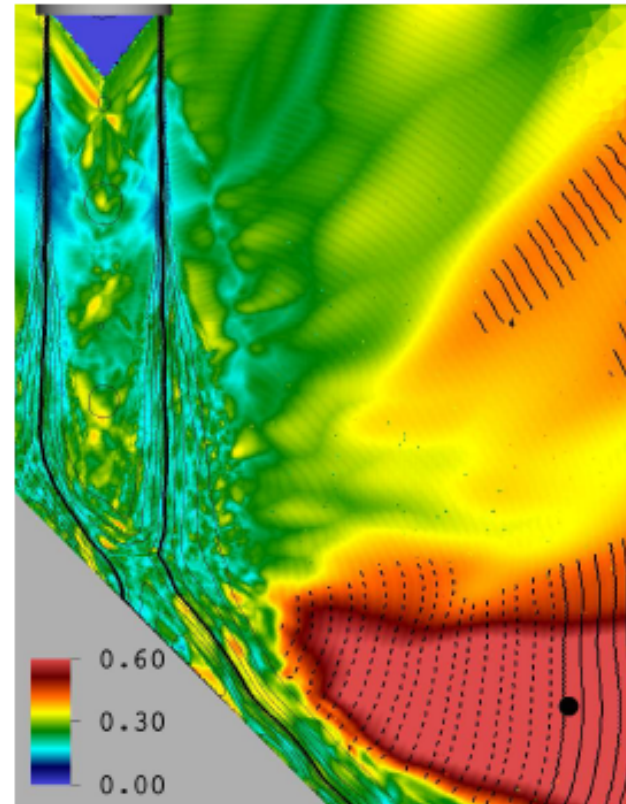
NORMALIZED CROSS-SPECTRAL DENSITY



$$\hat{C}_{p',\rho'Vr'Vr'}$$

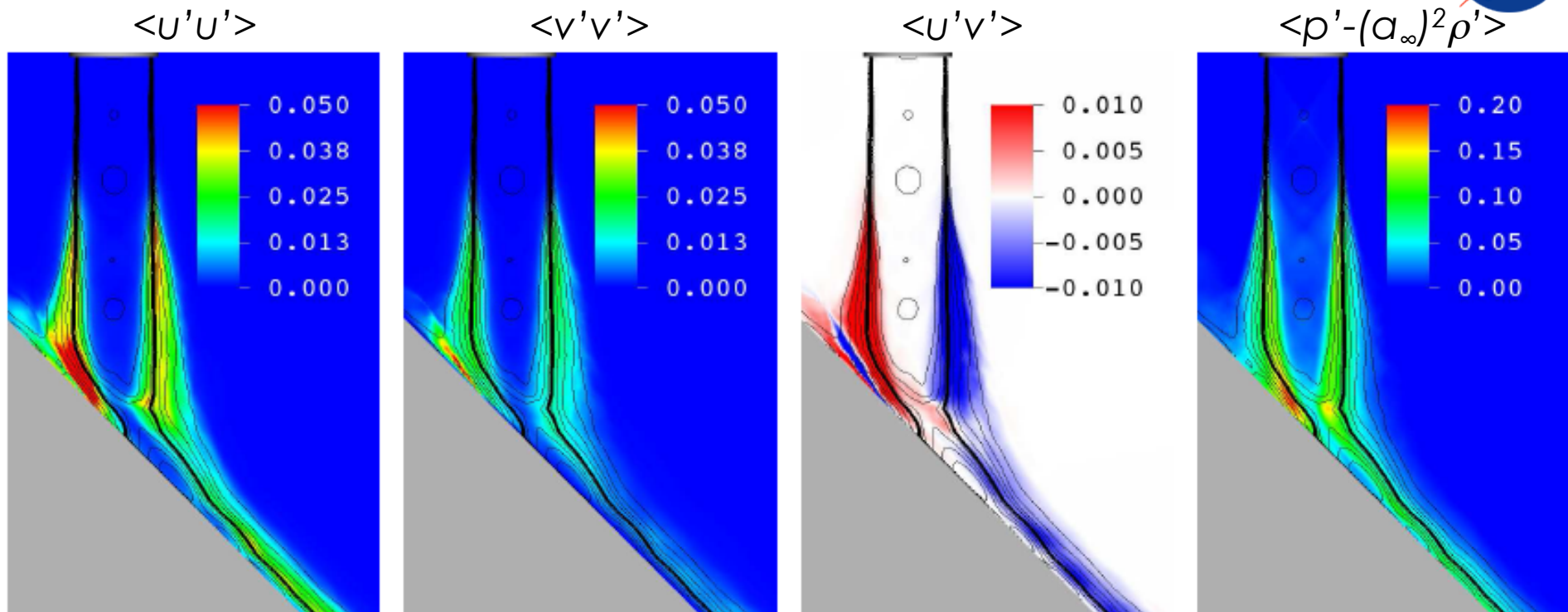


$$\hat{C}_{p',\rho'Vr'Vr'}$$



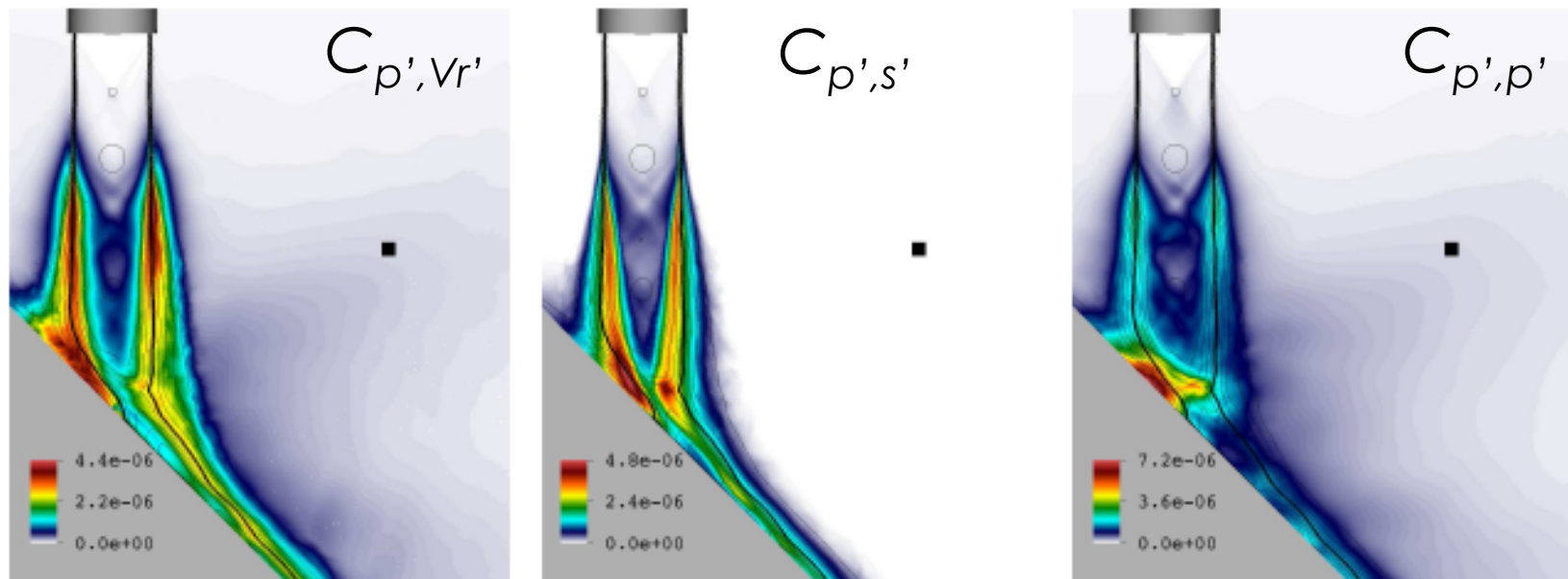
- Weak correlation of second-order terms (consistent with Panda (2005))
- Larger cross-spectral densities inside the jet for third order term
- No strong correlations can be observed for $\Theta=75^\circ$

REYNOLDS STRESSES



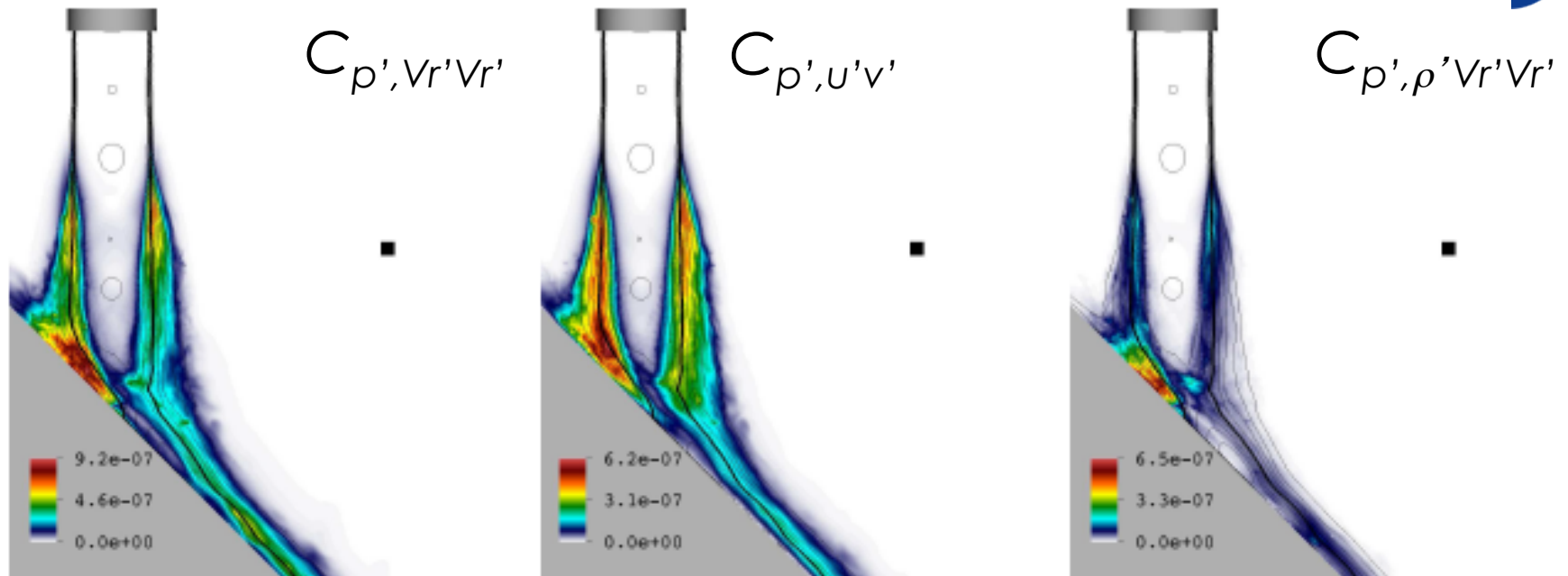
- Reynolds stresses provide an idea about regions with large unsteadiness but does not account for radiating part of the solution
- Slightly larger fluctuations in $\langle u'u' \rangle$ than in $\langle v'v' \rangle$ in the shear layer
- Velocity components were locally decomposed into streamwise (u) and cross-streamwise (v) flow directions
- Shear layer impingement region displays large fluctuation amplitudes
- Sign switch of $\langle u'v' \rangle$ right at shear layer impingement point
- $|p' - (a_\infty)^2 \rho'|$ shows largest values in shear layer and plate shock

UN-NORMALIZED CROSS-SPECTRAL DENSITY



- Small CSD values inside jet (potential core length $\sim 8D$)
- Amplitudes for un-normalized cross-spectral density is significant different from Reynolds stresses
- Peak for $C_{p',Vr'}$ occurs at the sonic line whereas peak for $C_{p',s'}$ occurs closer to the center axis
- Large values of $C_{p',Vr'}$ and $C_{p',s'}$ occur inside the wall jet's shear layer
- Large dipole contribution from $C_{p',p'}$ at shear-layer impingement point
- Distribution is only mildly affected by choice of observer point

UN-NORMALIZED CROSS-SPECTRAL DENSITY



- Higher-order terms display significantly lower amplitude
- Second and third-order terms display similar magnitudes
- Cross-spectral densities $C_{p',Vr'Vr'}$ and $C_{p',u'v'}$ highlight shear-layer impingement region
- $C_{p',\rho'Vr'Vr'}$ similar to $C_{p',\rho'}$ due to ρ'
- Subtle differences in un-normalized CSD and Reynolds stresses are due to including information about linear dependence for CSD



- Introduction to jet noise source identification and characterization
- Computational Simulation Strategy
- Characterization of Flow Field in Source Region
- Acoustic Wave Propagation Pattern
- Noise Source Identification
 - Causality Method
 - Proper Orthogonal Decomposition
- Discussion

PROPER-ORTHOGONAL DECOMPOSITION



- POD** results in a decomposition of the flow field into a set of basis functions that capture most of the flow energy as defined by a user-defined norm with the least number of modes*

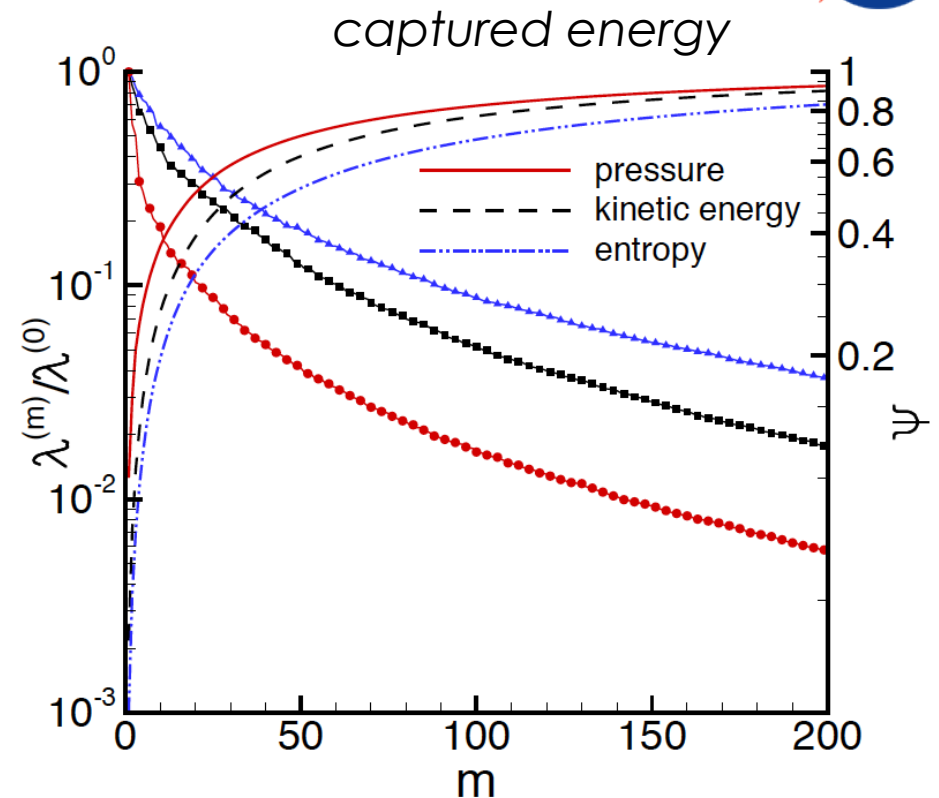
$$\vec{q}(\vec{x}, t) \approx \sum_{n=0}^I a^{(n)}(t) \vec{\chi}^{(n)}(\vec{x})$$

- Used snapshot method** in temporal domain
- Vector norm (energy) with

$$|\vec{q}|^2 = \int_V \left(\sum_{k=1}^{N_q} \omega_k q_k q_k \right) d\vec{x}$$

$q_k = [p, u, v, w, T^{0.5}]$ and weights ω_k .

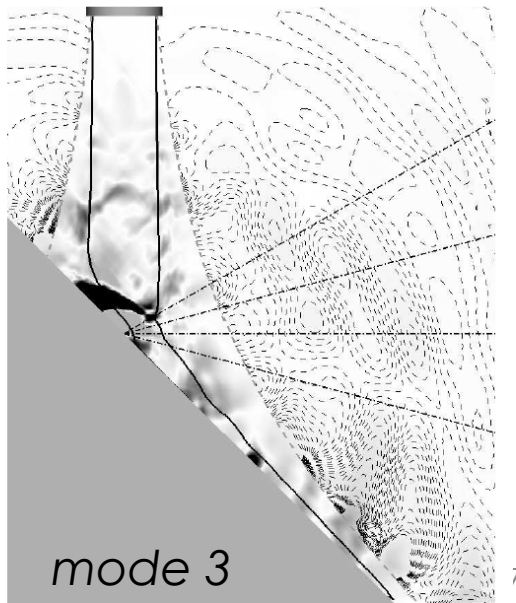
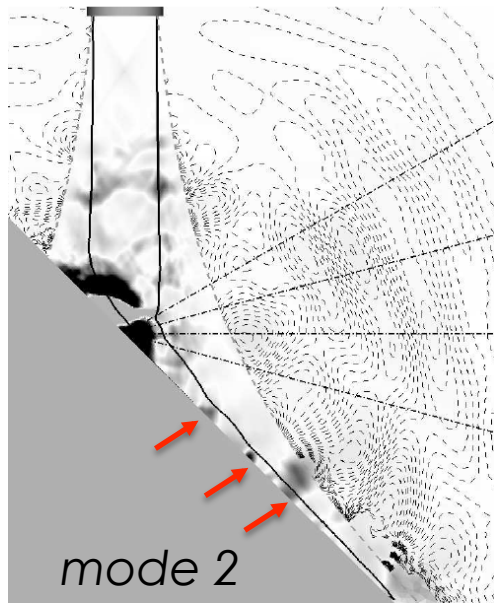
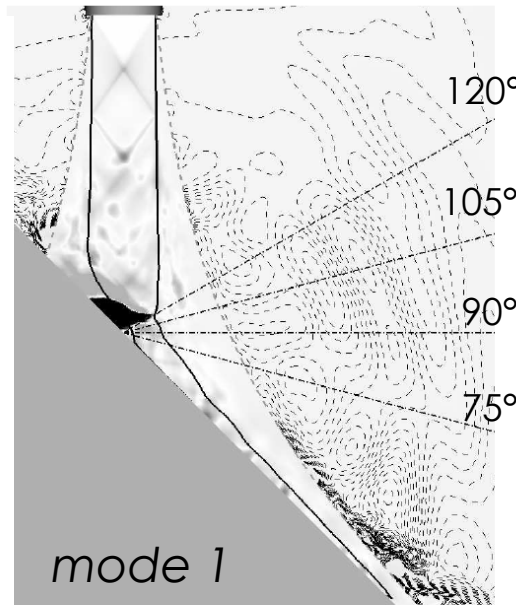
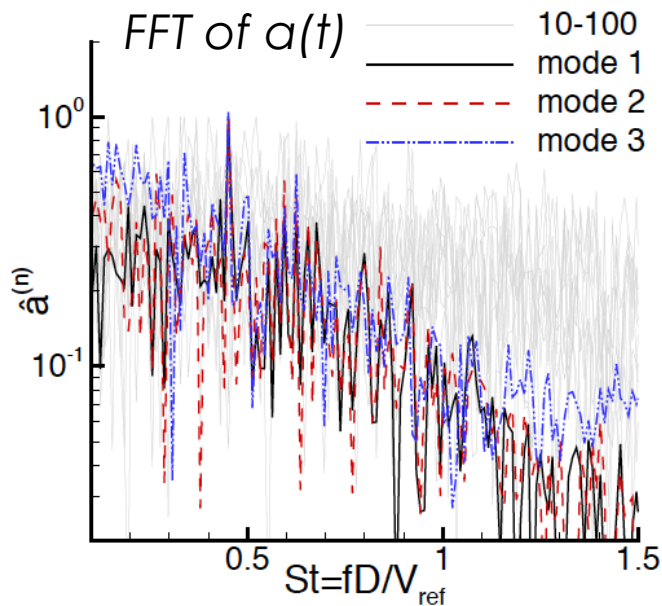
- Weights defined to use pressure, entropy, and kinetic energy



$$\text{with } \psi_N = \left(\sum_{n=1}^N \lambda^n \right) / \left(\sum_{n=1}^{N_{tot}} \lambda^n \right)$$

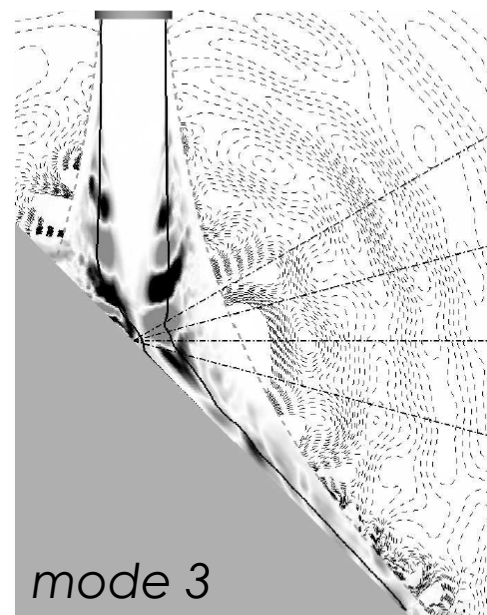
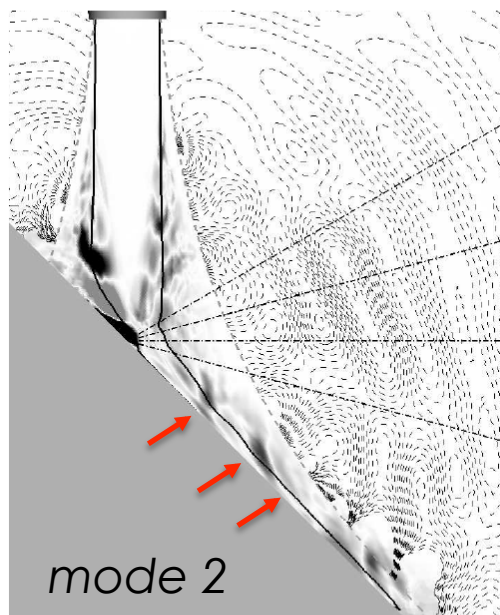
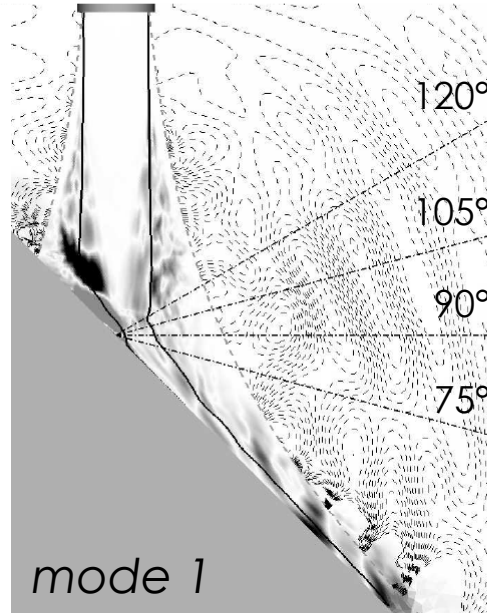
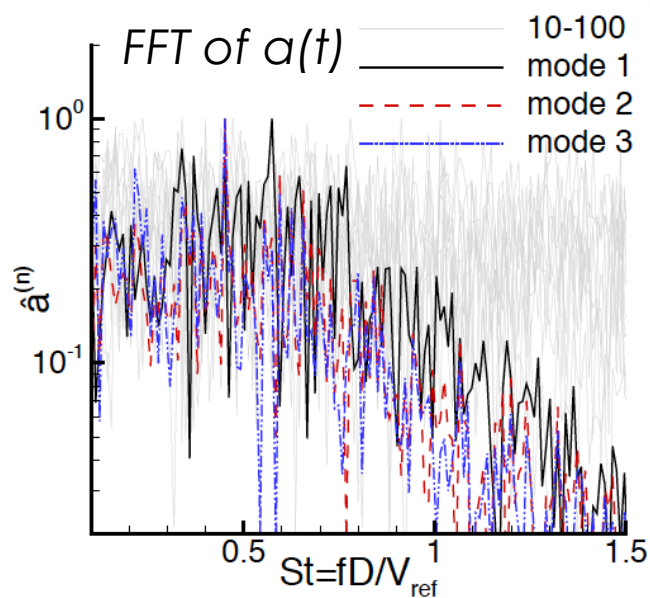
- Significant increase of coherence for jet impingement in comparison to free jets
- Pressure based POD shows strongest coherence

PRESSURE BASED POD MODES



- POD modes based on E_p pick up low ($St \approx 0.2$) and high ($St \approx 0.5$) frequency information
- Distributions portray the motion of the shocks (see also Brehm et al. (2013))
- Increased unsteadiness in the wall jet associated with tail shocks
- Two dominant wave propagation directions can be identified in dashed lines ("acoustic pressure field")

ENTROPY BASED POD MODES

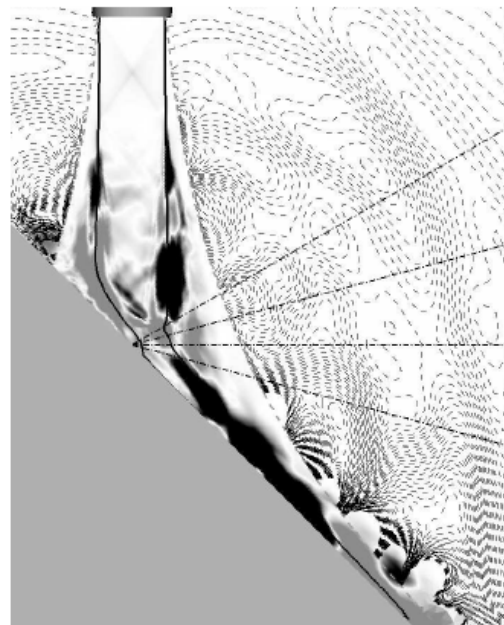
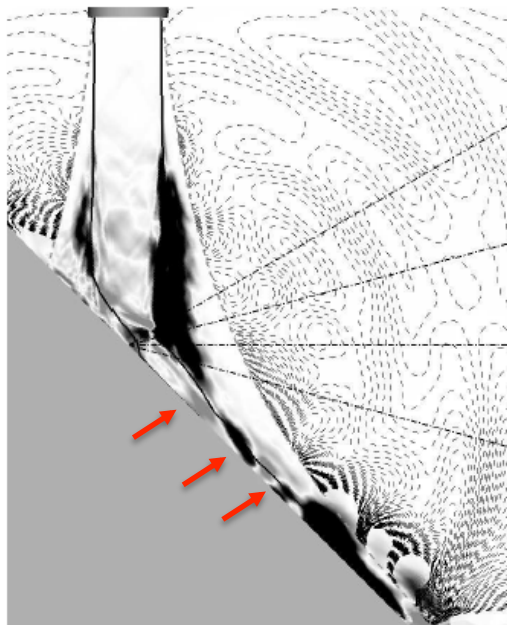
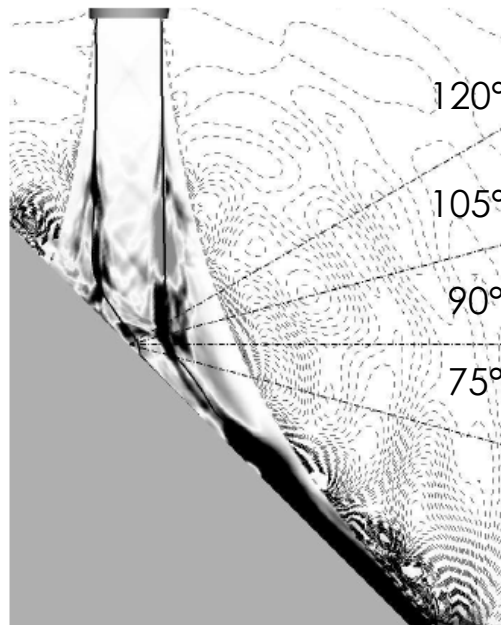
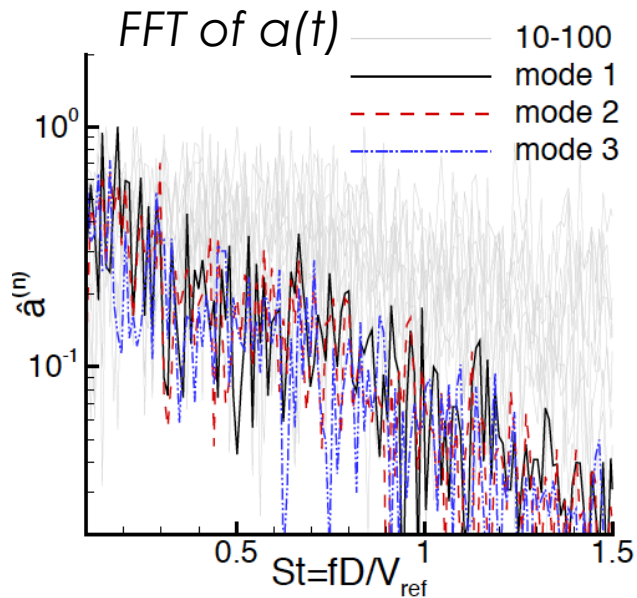


- Pressure field is obtained by projecting $p(t)$ onto right eigenvectors

$$\psi^{(n)}(\vec{x}) = \sum_{i=0}^N r_i^{(n)} q(x, t_i)$$

- POD modes based on E_s , show peaks around $St=0.4-0.6$
- Most energetic modes highlight vortex impingement (most dominant on the plate side)
- Some isolated peaks in the wall jet

KINETIC ENERGY BASED POD MODES



- POD modes based on E_s show peaks around $St=0.1-0.2$ ($\Theta=75^\circ$)
- Most energetic modes highlight wall jet and jet's shear layer away from the wall



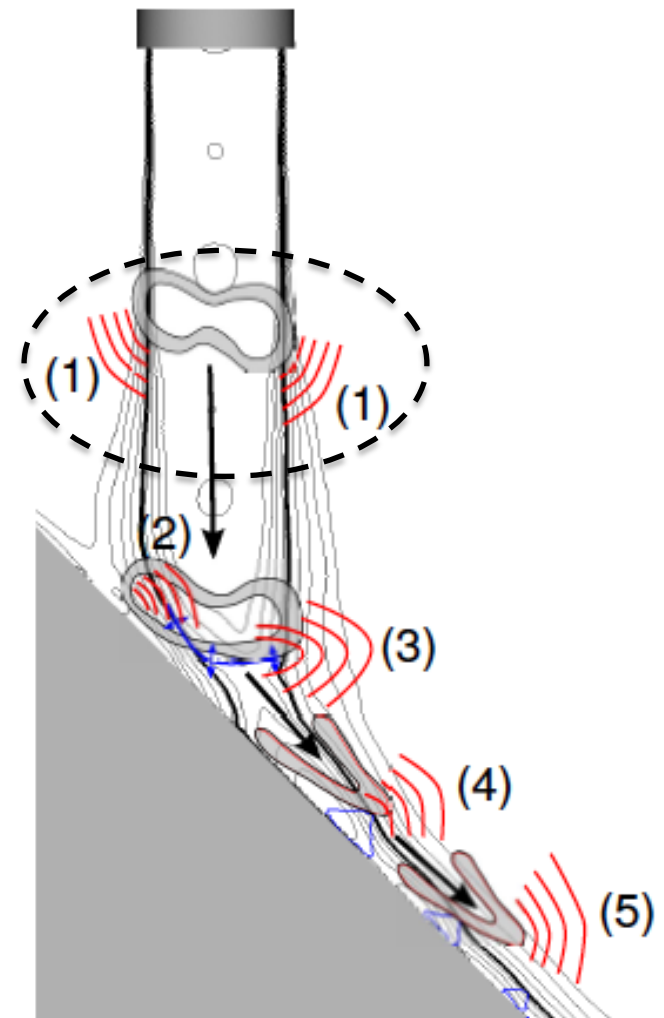
- Introduction to jet noise source identification and characterization
- Computational Simulation Strategy
- Characterization of Flow Field in Source Region
- Acoustic Wave Propagation Pattern
- Noise Source Identification
 - Causality Method
 - Proper Orthogonal Decomposition
- Discussion

DISCUSSION



- Noise generation was investigated following a three step approach:
 - Analysis of flow field in source region
 - Characterization of acoustic “far”-field
 - Connecting (1) & (2) employing causality method and POD
- Good comparison with experiments
- Quasi omni-directional noise generated by fine grained turbulence is left out (our methods are not appropriate for compact noise sources)
- Various indicator (such as Mach radiation or temperature contours) point towards existence of large scale turbulent structures in turbulent jet
- Coherent structures can be cross-correlated with acoustic pressure at $\Theta=120^\circ$ in jet axis centerline (large coherence length)
- Mach radiation **(1)**
- In addition to Mach radiation how are coherent flow structures involves in noise generation?

Illustration of possible noise sources



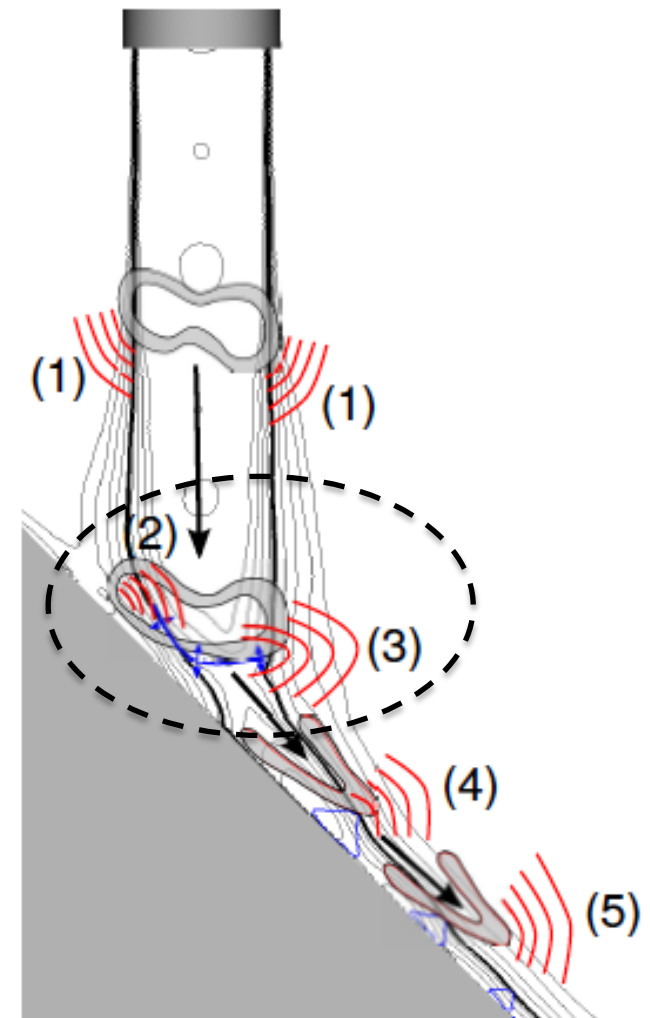
DISCUSSION



- Vortex sound theory can be used to explain that impinging vortices generate noise through stretching and tearing **(2)**
- Large Reynolds stresses and $C_{p',vr'}$ are associated with vortex impingement
- Most energetic POD modes based on the entropy fluctuation term visualize vortex solid wall interaction
- Dilatation contours and shock identification method displayed highly unsteady shocks in impingement and wall jet regions
- Large values of $C_{p',s'}$ around plate shock point towards shock associate noise **(3)**
- Pressure based POD modes visualize the unsteady motion of the plate shock
- For flows containing discontinuities, rewrite Lighthill stresses using generalized derivatives derivative:

$$\frac{\hat{\partial}^2 T_{11}}{\partial x^2} = \frac{\partial^2 T_{11}}{\partial x^2} + \frac{\partial}{\partial x} (\Delta T_{11} \delta(x - x_s)) + \Delta \left(\frac{\partial T_{11}}{\partial x} \right) \delta(x - x_s) \quad (\text{quadrupole, dipole, and monopole})$$

Illustration of possible noise sources

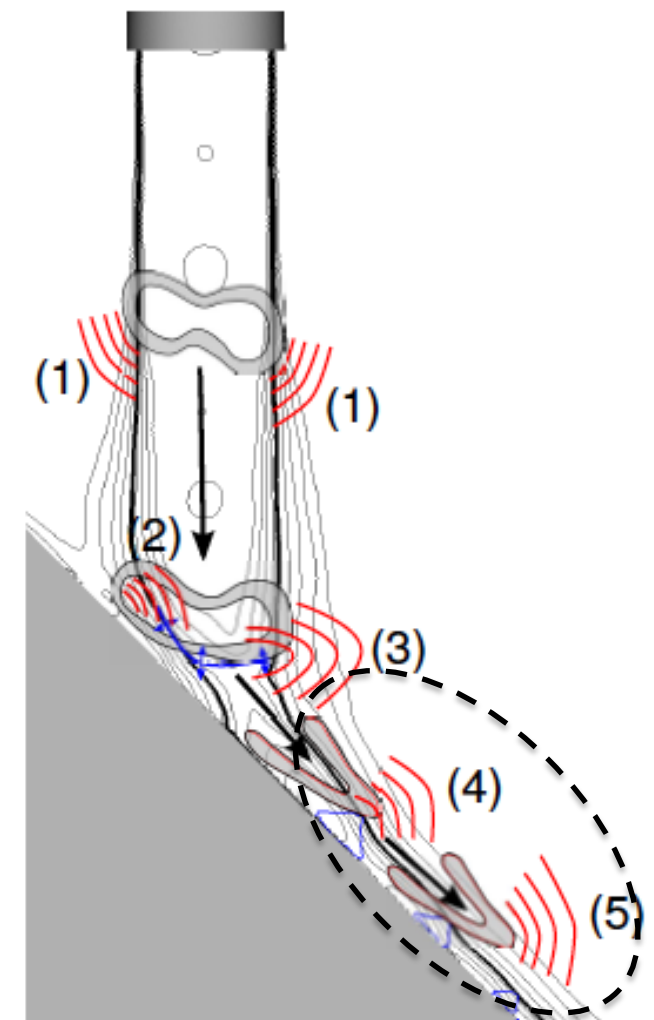


DISCUSSION



- Kinetic energy based POD modes pick up low frequency content observed in $\Theta=75^\circ$; large amplitudes in shear layer and wall jet
- How can we explain low frequency peak?
- Pressure based POD modes display large amplitudes for low ($St \approx 0.2$) and high ($St \approx 0.6$) frequencies; expected frequency of shock oscillations
- w' -frequency spectra displays low ($St \approx 0.2$) frequencies in impingement zone and standing wave in pressure spectra as well; may explain low frequency content in wall region
- Interaction of coherent flow structures with tail shocks may explain noise generation **(4)**
- St_{wall} computed with distance of tail shocks and speed of convective flow structures seems high
- Mach radiation from coherent flow structures play some role in noise generation (strong evidence in frequency-wavenumber plots) **(5)**

Illustration of possible noise sources



ACKNOWLEDGEMENTS



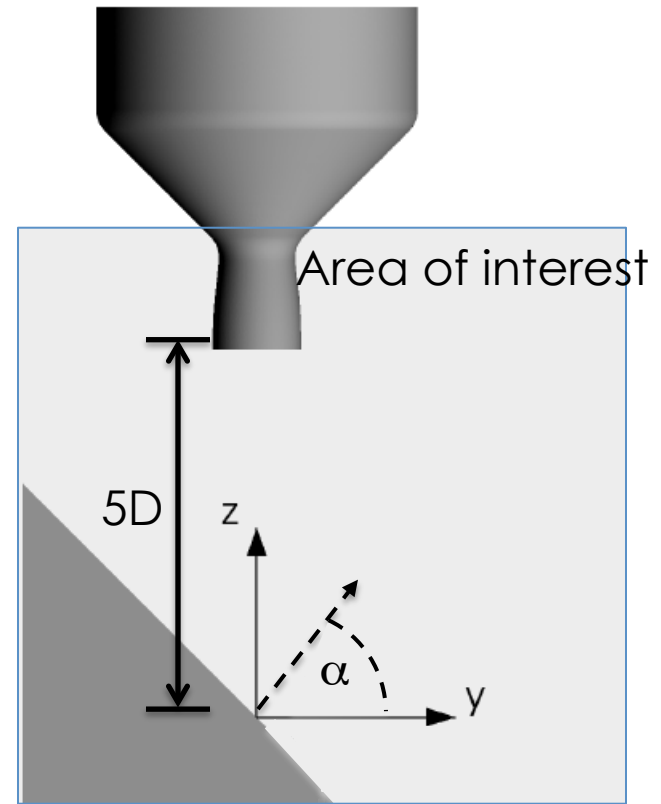
- LAVA group at Applied Modeling Simulations Branch, NASA Ames:
Dr. S. Moini-Yekta, Dr. M. Barad, and Dr. E. Sozer
- *Dr. M. Rogers and Dr. T. Manning* for useful discussions and valuable inputs to journal manuscript
- NASA Advanced Supercomputing (NAS) Division

particle tracing
core at the vorticity



Computational Setup

- Collaboration with JAXA**
- Conditions based on experiments by Nakanishi et al. at the UT-Kashiwa hypersonic and high-temperature wind tunnel*
- $M=1.8$, air at $T=300\text{K}$ (cold)
- $Re=V_e D/\nu=1.6 \times 10^6$
- 200-400 million grid points
- Nozzle-to-plate distance $5D$
- Impingement angle α



Flow conditions at nozzle exit and percent differences with perfectly expanded jet:

	Mach number	pressure, p_{ref} [Pa]	exit velocity, V_e [m/s]
exit conditions	1.8045	100,794	488.14
difference	~0.25%	~0.52%	~0.24%

*Tsubouchi et al. 2011, **Tsutsumi et al. 2012, **Nonmura et al. 2010 & 2011